DYNAMIC ANALYSIS OF ADOBE STRUCTURES

A Thesis

by

EDWARD JONATHAN SOTO OBLEA

Submitted to the Office of Graduate and Professional Studies of
Texas A&M University
in partial fulfillment of the requirements for the degree of

MASTER OF SCIENCE

Chair of Committee,	John Niedzwecki
Committee Members,	Joseph M. Bracci
	H. Joseph Newton
Head of Department,	Robin Autenrieth

May 2018

Major Subject: Civil Engineering

ABSTRACT

Adobe is an inexpensive material widely used in developing countries such as Peru. Its use as construction material does not demand expertise. Unfortunately, buildings constructed using adobe have a record of poor behavior when subject to strong ground motion. There are several ways to reinforce adobe buildings. For instance, black and nylon mesh can be introduced to improve the structural integrity. This research investigation studies the behavior of a one-story adobe building subjected to the 1970 Peruvian earthquake. Experiments were performed at the Catholic University of Peru (PUCP) and examined the undamaged and damaged conditions of a one-story adobe building. The experimental data from the phase 2 excitation case (60 mm maximum displacement) was analyzed and compared with ABAQUS models.

A variety of statistical and transform methodologies are available to study problems in structural dynamics and this study explores their use in modeling and characterizing the excitation and response of this building. A brief introduction regarding applications of Fourier and Wavelet transforms, and statistical methodology used in structural dynamics is presented. This is followed by a discussion of the mechanical properties of adobe building materials and the development of the ABAQUS building models. The data and the corresponding numerical predictions area characterized in terms of the frequency content, cross-correlation, Root Mean Square Error (RMSE) and Statistical peak ground acceleration (SPGA). The analysis results included estimates of the structural natural frequencies and corresponding modal information. In addition, PDF and CDF plots of the response behavior were used to characterize time series to compare the experimental measurements and the numerical simulations. Finally, both Fourier and wavelet analyses were used to characterize frequency content and the latter method was used to investigate time as well as relation to natural frequencies in the numerical models.

DEDICATION

The constant support from my beloved parents Angel and Gertrudis, as well as my brothers Miguel, Alvaro and Christian was fundamental to me as I pursued my studies at Texas A&M University. My former supervisors Dr. Marcial Blondet and Dr. Nicola Tarque, from the Department of Civil Engineering at the Catholic University of Peru (PUCP), have been important in my career direction and I am most grateful for their references to study in the US.

ACKNOWLEDGEMENTS

I am most grateful for the funding that I received from the Fulbright Scholarship Program in Peru and LASPAU: Academic and Professional Program for the Americas managed through Harvard University that allowed me to pursue my studies and research at Texas A&M University. The sharing of the unique one-story adobe building response data from the experimental research conducted at the Catholic University of Peru (PUCP) by their faculty in the Department of Civil Engineering was central to my thesis research and permission to use this data in my thesis research was very much appreciated.

I would like to thank my committee chair, Dr. Niedzwecki, for his guidance and support throughout the course of this thesis research investigation. Further, the technical comments provided by my committee members, Dr. Bracci and Dr. Newton, are gratefully acknowledged. My thanks also go out to my friends and the department faculty and staff for making my time at Texas A&M University a good experience.

Finally, I would like to thank to my father, mother, and brothers for their encouragement, patience, and constant support throughout this journey.

CONTRIBUTORS AND FUNDING SOURCES

This work was supervised by the thesis committee consisting of Professor John M. Niedzwecki (thesis advisor) and committee members Professor Joseph M. Bracci of the Zachry Department of Civil Engineering, and Professor H. Joseph Newton from the Department of Statistics.

Professors Dr. Marcial Blondet and Dr. Nicola Tarque, provided the experimental time series data that was analyzed as part of this thesis research. The data was part of an experimental study in which I participated with these professors that was conducted at the Catholic University of Peru (PUCP).

All of the research work conducted and reported in this thesis was completed by the student independently.

This graduate study was supported by a fellowship from the Fulbright Program in Peru and LASPAU: Academic and Professional Programs for the Americas.

TABLE OF CONTENTS

Page

LIST OF FIGURES

Page

LIST OF TABLES

Page

1 INTRODUCTION

1.1 Fourier and Wavelet Transforms in Structural Dynamics

Several methods in Structural Dynamics are available to help us interpret the behavior of structures subjected to earthquake motion. Both time domain and frequency domain analysis methods are widely used, but they are not effective in analyzing variations of power or frequency content variation in time. A more recent development, Wavelet analysis provides a powerful tool that can be utilized to analyze time series. Fourier transforms the entire duration of a signal; however, there is no way to detect if a local frequency oscillation occurring at several frequencies located throughout the entire signal or just at a certain period. This limitation is overcome by means of the Wavelet analysis, which divides a signal into its constituent parts (Newland, 1996).

Time history analysis methods are most commonly used to interpret recorded earthquake signals of structures. However, parameters such as stiffness and critical damping ratios can vary depending on the frequency content. The typical Fourier Transformation (FT) methods are best used to understand the behavior of linear systems in the frequency domain (Clough and Penzien, 1995). Thus, this method is not adequate alone when trying to evaluate variations in frequency content (Bradford, Yang, and Heaton, 2006). Real earthquake activity results in structural response behavior that encompasses nonlinear behavior, variations in frequency content and dynamics parameters, and structural damage. Thus, frequency/time domain methods help understand the dynamic behavior of structures and can aid in the detection of possible structural damage.

Time/frequency domain models have been developed, as shown in Figure 1.1. These methods include the time domain, frequency domain, Short-time Fourier Transformation (STFT), and wavelet analysis. The time domain model characterizes the signal while frequency domain methods reveal important information regarding frequency content and frequency-dependent amplitude (Montejo and Suarez, 2006). The STFT can be used to reveal frequency/time methods assuming linear behavior. Wavelet methods are an extension of the Fourier method and are suitable to study nonlinear systems, while stochastic dynamic analysis can contribute to a better understanding via obtain power spectra (Politis, 2000). Non-linear behavior of structures can be analyzed by means of time/frequency methods. Research has shown that time domain methods and frequency domain methods alone do not always provide adequate results to interpret complex behavior. Combined frequency-time studies are recommended for earthquake applications, especially to detect changes in frequency content and damage (Politis et al, 2000).

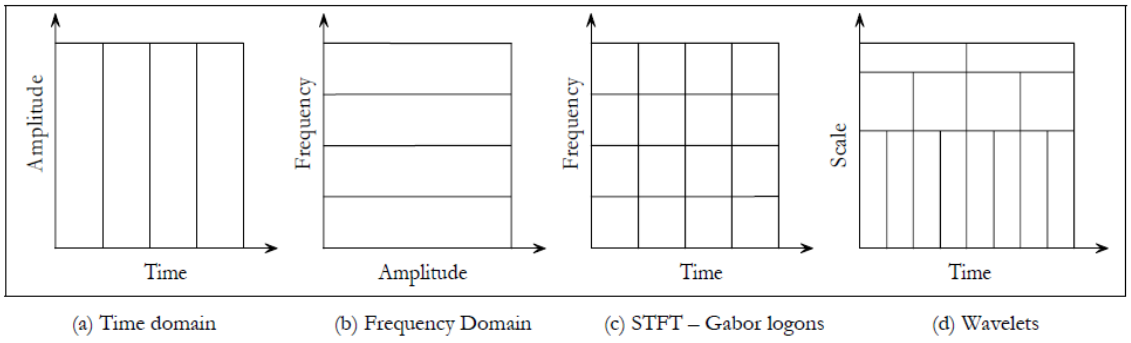

Figure 1.1. Time and frequency models' representations (Reprinted from Politis, 2000).

Several time-frequency methods based on Fourier transform have been developed such as the Wavelet and Wigner-Ville transform. The energy distribution by means of the Wavelet Transform method was studied according to different scales after the 2001 (Moment Magnitude: Mw = 8.4) Chilean earthquake (Boroschek and Comte, 2004). The evolution of the frequency content with the Wigner-Ville Transform (WVT) was studied on both linear and nonlinear models subjected to synthetic earthquakes on a twenty-story building and the Millikan Library on Caltech campus. The WVT numerical analysis provided an estimation of the damage of the structures after severe earthquake (Bradford, Yang and Heaton, 2006). Using the WVD transform method provided insight into signal interferences due to its quadratic nature, while traditional methods such as the short time Fourier transform have difficulties with having fixed windows (Li et al. 2009). In addition, the WVD and SFT methods provide more information that is needed and computations might take long time (Newland, 1996). The Wavelet Transform (WT) has appeared as tool that overcomes those drawbacks and has several advantages. It can help identify data segments for analysis in which important information can be hidden. Another great advantage is that it requires less computational effort compared to the Wigner Ville Method. Moreover, the Wavelet transform can be used in the detection of progressive damage in structures considering both linear and nonlinear FEM analysis. (Li et al. 2009). This feature is very important for Structural Health Monitoring.

Regarding the power spectral density (PSD), it provides a reduction in the signals. However, further reduction is sometimes necessary for a better extraction of signals characteristics. Spectral moments have been widely used in this reduction and applied to stationary random processes such as vocal range, ocean wave, and fatigue failure analysis

(Alamdari et al. 2016). This research will focus on the application of wavelet and power spectral density analysis to investigate the response of adobe masonry structural design.

1.2 Building materials

Adobe is one of the oldest building materials and it is widely used in regions such as Latin America, The Middle East, and northern-and-southern Africa. In Peru, adobe dwellings comprise around 40% of total buildings, especially in rural areas where sometimes is the only material available for construction (Bariola and Sozen, 1990). Adobe is widely used because of its cost, availability, good thermal and acoustic isolation (Tarque et al. 2014). There are several important dynamic properties regarding adobe as construction material and that contribute towards to high seismic vulnerability. First, adobe masonry walls are heavy and engender great inertial forces. Second, adobe masonry is a relatively weak structural material and therefore cannot resist these great forces. In addition, adobe is a brittle and fragile material; it can collapse suddenly without warning (Blondet et al. 2006).

Figure 1.2. Typical adobe buildings in the world.
A) One story dwelling in Iran (Reprinted from Kumar, 2002). B) Two-story adobe building in Cusco, Peru (Reprinted from Blondet, M. et al. 2004).

Nylon is an inexpensive material that is widely available in rural areas. It is also easy to incorporate it for wall reinforcement; it does not require any special expertise (Blondet et al. 2017). One important parameter to take into account is the diameter of the nylon string. In fact, wall covering constrains the string diameter for construction. E080 Adobe Peruvian code states that covering should be between 15 and 20 mm. In Peru, it is recommended to use 5/32" nylon strings for reinforcement due to its availability in poor areas (Mattson, 2015). The modulus of Elasticity for nylon strings obtained from experimentation is E = 60 MPa (Blondet et al. 2017).

The concrete ring foundation was used to transport the adobe model from construction site to the shaking table test. The modulus of Elasticity of concrete is E = 20 GPa.

There are several studies regarding the material properties of adobe. For instance, the adobe masonry properties were used in a numerical nonlinear model regarding damaged plasticity (Tarque et al. 2014).

Table 1.1. Material properties for adobe masonry (Reprinted from Tarque et al. 2014).

Elastic			Tension		Compression	
E (MPa)	υ	ϒ (N/mm^3)	f_t (MPa)	G_f (N/mm)	f_c (MPa)	G_f (N/mm)
200	0.20	$2x10^{-5}$	0.04	0.01	0.45	0.16

Where E is the modulus of elasticity; υ is the Poisson ratio; ϒ is the volumetric weight, f_t is the tensile strength; f_c is the compressive strength; and G_f is the fracture energy.

The mechanical properties of adobe material can be obtained by means of dynamic tests such as the typical simple compressive and diagonal compressive tests (Silveira et al. 2015). Figure 1.3 shows these two typical tests on laboratory.

Figure 1.3. Typical tests on adobe masonry. A) Simple compression. B) Diagonal compression (Reprinted from Blondet, M. et al. 2015).

The compressive tests bring about typical mechanical properties of adobe material as presented by Silveira (2015); the results are shown in Table 1.2.

Table 1.2. Material properties for adobe masonry (Reprinted from Silveira et al. 2015).

Simple Compression			Diagonal Compression	
E (MPa)	υ	f_c (MPa)	f_s (MPa)	G (MPa)
750	0.16	0.33	0.026	0.41

Where E is the modulus of elasticity, f_c is the compressive strength, f_s is shear strength; and G is the modulus of rigidity. In fact, the values are similar regarding the study performed by Tarque (2014). Nonetheless, there is some discrepancy regarding the modulus of Elasticity.

For adobe structures, the yield criterion is recommended to obtain a nonlinear stress-strain constitutive law; nonlinear expressions consider the reduced strength of adobe material representing softening and hardening plots. An exponential model for uniaxial tension and

parabolic expression for uniaxial compression is recommended for analysis. Figure 1.4 shows the constitutive stress-strain law which were obtained from mechanical tests and recommended to model the nonlinear behavior of adobe material (Tarque et al. 2014).

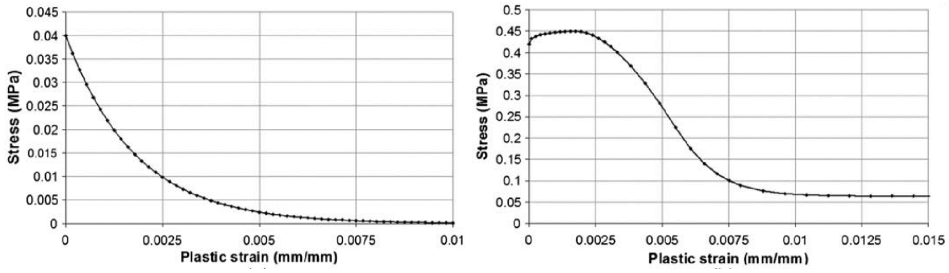

Figure 1.4. Constitutive stress- strain-law for adobe material. Left: uniaxial tensile behavior. Right: uniaxial compressive behavior (Reprinted from Tarque et al. 2014).

Over the years, there has been many tests on full-scale adobe buildings to study the behavior of reinforced and unreinforced earthen dwelling subjected to seismic activity. For instance, a full-scale adobe model, whose walls were reinforced with nylon strips, was tested on the shaking table of the Structural Laboratory of the Catholic University in Peru (PUCP). Nylon strings were used for vertical and horizontal reinforcement in adobe structures which were subjected to seismic excitation. The reinforcement was deemed to be good because it provided additional structural strength and avoided the total collapse of adobe walls (Blondet et al. 2017). Biaxial geogrid mesh was also considered on the reinforcement of adobe dwellings. However, the nylon strips provided an inexpensive and easily available solution (Figure 1.5).

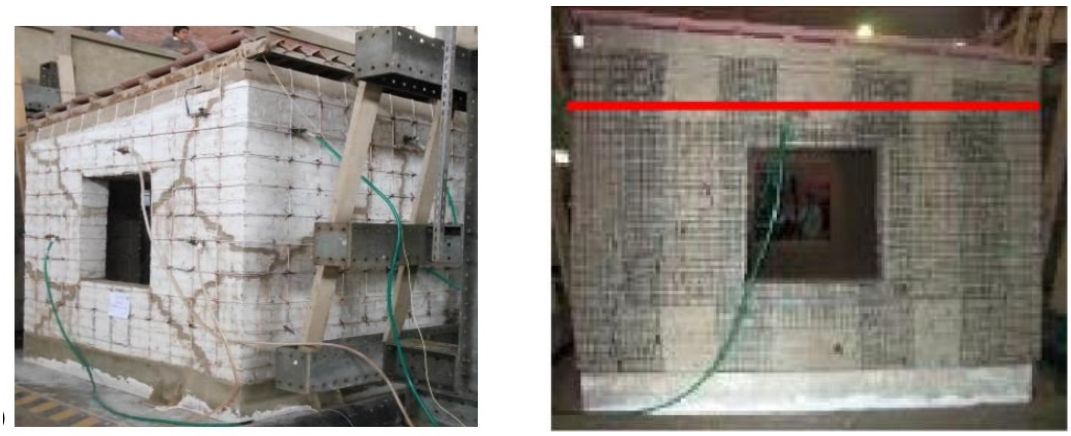

Figure 1.5. Reinforcement on adobe full-scale models. A) Nylon strip. B) Biaxial geogrid mesh (Reprinted from Blondet al. 2017).

1.3 Research objectives

The primary objective of this research is to analyze the response behavior of a typical one-story adobe dwelling subjected to seismic simulation which represents random excitation (strong ground motion). In particular, the focus is on comparing the results obtained from experimental data and the ones brought about by ABAQUS software. The data content gives relevant information: implications from statistical pdf and cdf plots, spectral content obtained from Fourier analysis, and the use of wavelet transforms to discern trends in time-frequency analysis. Provided that adobe is an inexpensive material widely used in rural areas of developing countries such as Peru, literature survey of adobe as building material and experiment tests were pursued in this research. For instance, seismic simulations on full-scale adobe models are presented. Thus, mathematical formulation involving Fourier approach and Wavelet Transform as well as Statistical analysis is presented. Afterwards, a one-story adobe building structure was studied; it was subjected to seismic simulation at the Catholic University of Peru; cracks appeared in the building. The dwelling was retrofitted and then subjected to a second seismic simulation. Accelerometers and linear variable displacement

transducers were installed to monitor the structural behavior of the building in both experiments. These devices provided time domain results for both the undamaged and retrofitted adobe model. Hence, ABAQUS software was used to model both the original and repaired adobe structure. The results from experiments and ABAQUS numerical simulations were used to generate statistical plots, estimate natural frequencies and modes for the undamaged model, and provide spectral and wavelet analysis.

2 MATHEMATICAL FORMULATION OVERVIEW

2.1 Fourier Approach

Any arbitrary load function can be expressed in terms of periodic terms by means of the Fourier series representation. Figure 2.1 shows an arbitrary load which was extended by means of a period 'Tp'; this procedure brings about artificial load. As 'Tp' increases and tends to infinite, the spurious function disappears (Clough and Penzien, 1995).

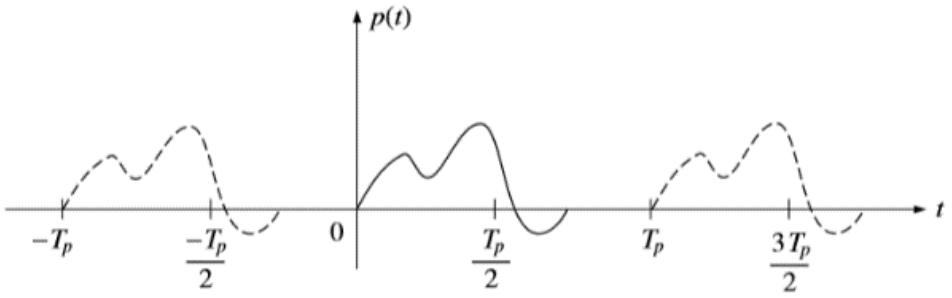

Figure 2.1. Arbitrary load represented by Fourier series (Reprinted from Clough and Pienzen, 1995)

The inverse and direct Fourier transformations can be expressed in terms of the continuous frequency function $\bar{\omega}$. Clough (1995) presents these equations.

$$p(t) = \frac{1}{2\pi}\int_{-\infty}^{+\infty} P(i\bar{\omega})e^{i\bar{\omega}t}d\bar{\omega} \tag{2.1}$$

$$P(i\bar{\omega}) = \int_{-\infty}^{+\infty} p(t)e^{-i\bar{\omega}t}dt \tag{2.2}$$

Where $\boldsymbol{P}(i\bar{\omega})/2\pi$ stands for the complex amplitude at frequency $\bar{\omega}$ per unit of $\bar{\omega}$.

An important definition is the Fourier Amplitude Spectrum which can be expressed by means of the classical Fourier Series transformation. The following equation represents the definition (Sokolov, 2002).

$$X(f) = \int_{-\infty}^{+\infty} x(t) e^{-2\pi i f t} dt = |X(f)|\, e^{-i\phi(f)} \quad (2.3)$$

Where X(f) is the Fourier amplitude spectrum related to time series signal x(t); $\phi(f)$ is the phase spectrum.

Regarding a signal such as earthquake motion, the Direct Fourier Transform (DFT) is recommended. Figure 2.2 shows the discretization of an arbitrary loading sampled at N points; the n value varies from 0 to N-1; the N value is usually an integer power of 2 (Barroso, 2017).

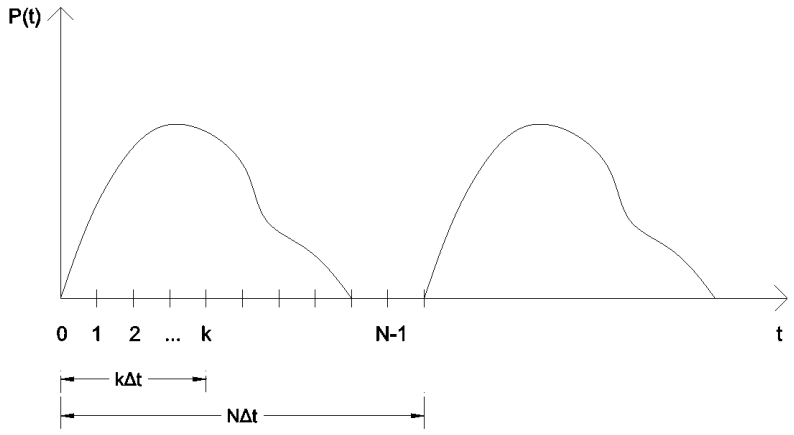

Figure 2.2. Discretization of a non-periodic force (Reprinted from Barroso, 2017)

There are multiple forms to express the DFT of the load. One common way is shown.

$$P(\Omega) = P(n\Delta\Omega) = \sum_{k=0}^{N-1} p(k\Delta t) e^{\left(\frac{-2\pi i k n}{N}\right)} \Delta t \quad (2.4)$$

Where the $\bar{T}$ period is defined by

$$\bar{T} = N\Delta t = \frac{2\pi}{\Delta\Omega} \tag{2.5}$$

The DFT of the unit impulse function can be expressed similarly.

$$\mathrm{H}(\Omega) = H(\mathrm{n}\Delta\Omega) = \sum_{k=0}^{N-1} h(k\Delta t) e^{\left(\frac{-2\pi i k n}{N}\right)} \Delta t \tag{2.6}$$

Then, the structural response in the frequency domain is obtained

$$X(\Omega) = H(\Omega) * P(\Omega) \tag{2.7}$$

$$X(\mathrm{n}\Delta\Omega) = H(\mathrm{n}\Delta\Omega) * P(\mathrm{n}\Delta\Omega) \tag{2.8}$$

Afterwards, the response in the time domain x(t) can be assessed by means of the Discrete Inverse Fourier Transform related to the response.

$$\mathrm{x(t)} = x(\mathrm{k}\Delta\mathrm{t}) = \sum_{k=0}^{N-1} X(\mathrm{n}\Omega) e^{\left(\frac{2\pi i k n}{N}\right)} \Delta\Omega \tag{2.9}$$

The amount of computation effort required by the DFT is greatly reduced by means of the Fast Fourier Transformation (FFT) which can work with any arbitrary N quantity. For instance, if $N=2^{10}$, the FFT method requires only 0.5% of computational effort related to standard assessment (Chopra, 2007).

2.2 Wavelet approach

Identifying dynamic properties such a stiffness and critical damping ratio is really important to understand the response behavior and possible damage in the structure. Time – frequency representation (TFR) such as the Wavelet transform allows identification of separation of these components taking into account time and frequency domains. A wavelet is a real or

complex oscillatory function which is located on both time and frequency domain (Gaviria and Montejo, 2017). In fact, one disadvantage of the DFT and FFT methods is that they do not show time resolution. The Wavelet tools methods allow local analysis of signals; a desired time interval can be zoomed and analyzed (Ghodrati et al. 2009).

A wavelet function W(x) can be defined by means of a dilatation function which expands horizontally a determined function. For instance, $\phi(x)$ can represent the dilatated version of $\phi(2x)$; $\phi(x)$ has the same height but is extended twice the horizontal scale of x. The following equation defines the wavelet function equation (Newland, 1996):

$$W(x) = -c3\phi(x) + c2\phi(2x-1) - c1\phi(2x-2) + c0\phi(2x-3) \quad (2.10)$$

Where c0, c1, c2 and c3 are numerical constants; they take positive and negative values. This set of coefficients must satisfy properties such as unit area, accuracy and form an orthogonal wavelet system; these properties are expressed in the following equations:

$$\sum_{k=0}^{N-1} c_k = 2 \quad (2.11)$$

$$\sum_{k=0}^{N-1} (-1)^k k^r c_k = 0; r = 0,1,2 \dots, N/2-1 \quad (2.12)$$

$$\sum_{k=0}^{N-1} c_k c_{k+2r} = 0; r \neq 0 \ and \ r = 1,2 \dots, N/2-1 \quad (2.13)$$

There are two types of Wavelet transform that have been used especially for dynamic identification purposed. The most common is the Complex Morlet Wavelet (Grossman, A. and Morlet J., 1984). The following equation expresses the formulation which is clearly an exponential decay.

$$\psi_{ComplexMorlet}(t) = (\pi f_b)^{-0.50} e^{2\pi j f_c - t^2/f_b} \quad (2.14)$$

Where f_b is the frequency bandwidth; f_c is the central frequency related to the mother wavelet function. The other commonly used wavelet is the Gabor transformed defined as it follows.

$$\psi_{Gabor}(t) = (\pi\sigma^2)^{-0.25} e^{\eta j t - t^2/(2\sigma^2)} \quad (2.15)$$

Where σ is the frequency bandwidth; η is the central frequency related to the mother wavelet function. The two wavelet approaches are similar regarding exponential decay; they are proportional and there is no advantage regarding using one or another in the Continuous Wavelet Transform (CWT) method (Gaviria and Montejo, 2017).

One of the most common Wavelet Transform tools that are used to identify dynamic properties is the Continuous Wavelet Transform (CWT). The CWT works with two Morlet mother functions: the complex Morlet and the Gabor Wavelet. CWT is defined as a convolution of the signal x(t) and the short/amplified version of mother wavelet ψ.

$$\psi_{a,b}(t) = \frac{1}{\sqrt{a}} \psi\left(\frac{t-b}{a}\right) \quad (2.16)$$

$$WT(a,b) = \int_{-\infty}^{+\infty} x(t)\psi_{a,b}(t)dt \quad (2.17)$$

Where WT is the matrix of wavelet coefficients related to 'a' scale and 'b' time location. The mother wavelet function should be chosen carefully for success in the analysis. (Gaviria and Montejo, 2017). The mother wavelet function should take into account two conditions: neutral mean and limited energy. These conditions are expressed in the following equations, respectively.

$$\int_{-\infty}^{+\infty} \psi_{a,b}(t)dt = 0\,; \int_{-\infty}^{+\infty} \left|\psi_{a,b}(t)\right|^2 dt < \infty \quad (2.18)$$

On the other hand, the Discrete Wavelet algorithm is used to solve the compute the coefficients:

$$a_0 = \int_0^1 f(x)\phi(x)dx \tag{2.19}$$

$$a_{2^j+k} = 2^j \int_0^1 f(x)W\left(2^j x - k\right)dx \tag{2.20}$$

Where f(x) is a periodic signal; $\phi(x)$ is the scaling function; and $W(2^j x-k)$ are the wavelet functions related to the interval $0<x<1$. Hence, the former coefficients should follow the orthogonality properties.

After choosing a wavelet function, it is important to define a set of scales. The sets are discrete for orthogonal scales; these sets are arbitrary for not orthogonal wavelet, though. It is recommended to expressed scales in terms of power of two (Torrance and Compo, 1998).

$$s_j = s_0 2^{j\delta_j}; j = 0,1,\dots,J \tag{2.21}$$

$$J = {\delta_j}^{-1}\log_2(N\delta t/s_0); j = 0,1,\dots,J \tag{2.22}$$

Where s_j and J are the smallest and largest possible scale, respectively; δ_j is the factor for scaling (it is usually 0.50 for Morlet Wavelet and could have greater values for other wavelet functions); and N is the number of points.

In addition, MATLAB's CWT method relies on an expansion of an integral related to a time interval j and x(j) fixed for analysis.

$$WT(a,b) = \frac{1}{\sqrt{a}}\sum_j x(j)\left(\int_{-\infty}^{j+1}\psi\left(\frac{t-b}{a}\right)dt - \int_{-\infty}^{j}\psi\left(\frac{t-b}{a}\right)dt\right) \tag{2.23}$$

The program evaluates the former equation by means of assessing just once the integrals. In addition, a discrete number of points in the analysis is considered by means of a precision

parameter. If this parameter increases, a better discretization and therefore enhanced computation work is obtained (Gaviria and Montejo, 2017).

2.3 Statistical characterization

Spectral Moment

Spectral moments are parameters that recover information directly from the Fourier Spectrum without any further manipulation; they are useful for nonstationary stochastic methods. As a matter of fact, they can characterize signals which are covered in Gaussian process such as a noise environment. The spectral moments up to the 4th order give information about the process; higher order moments are generally not useful (Alamdari et al. 2016). The nth spectral moment related to a sensor at location j and Power Spectral Density (PSD) of the response (S_{xx_j}) can be expressed by the following equation.

$$\lambda_{x_j}^n = \int_{-\infty}^{+\infty} |\omega|^n S_{xx_j}(\omega) d\omega \tag{2.24}$$

For a discretized signal, the nth spectral moment can be expressed by

$$\lambda_{x_j}^n = \frac{2}{N^{n+1}} \sum_0^{0.5N} S_{xx_j}(k) \left(\frac{k}{dt}\right)^n ; 1 \leq j \leq 0.50N \tag{2.25}$$

Where S_{xx_j} is the discrete double-sided spectral density with N points, and dt is the sampling period for the referred signal.

Theoretical spectrum and significance levels

An appropriate background spectrum is required to determine significance levels. For geophysical phenomena background spectrum, it is recommended to use white noise (with flat spectrum) or red noise (with decreasing frequency and increasing power spectrum). The discrete Fourier spectrum can be modeled and normalized according to autoregressive process (Torrence and Compo, 1998):

$$P_k = \frac{1-\alpha^2}{1+\alpha^2-2\alpha\cos(2\pi k/N)}; k = 0,1,\ldots,N/2 \quad (2.26)$$

where P_k is the Fourier Power Spectrum; α is the lag-1 autocorrelation. An appropriate correlation brings about a red-noise spectrum; α=0 induces a white-noise spectrum.

Significance levels are associated with terms such as confidence intervals and null hypothesis. For example, a 95% confidence-interval is related to a confidence range about a determined value. In addition, the null hypothesis is a statement that would be tested. For instance, a null hypothesis for wavelet spectrum assumes that the time signal has a mean power spectrum if a peak in the wavelet spectrum is significantly above the background spectrum. The distribution for the Wavelet distribution can be expressed as it follows:

$$|W_n(s)^2|/\sigma^2 \rightarrow 0.50P_k\lambda^2 \quad (2.27)$$

where Wn(s) is the wavelet power spectrum related to time n and scale s.

In addition, the boundary terms for the confidence interval for $Wn^2(s)$ is expressed.

$$\frac{2}{\lambda^2(0.50p)}|W_n(s)|^2 < \mathrm{Wn}^2(\mathrm{s}) < \frac{2}{\lambda^2(1-0.50p)}|W_n(s)|^2 \quad (2.28)$$

where p is the significance level (p = 0.10 represents a 90% confidence interval); λ^2 is the chi-square distribution evaluated at 0.50p and 1- 0.50p.

Wavelet smoothing can be done according to time averaging and scale averaging. Smoothing the wavelet spectrum in time scale provides some advantages. First, Fourier spectrum approximates the wavelet spectrum; the amount of necessary smoothing decreases as scale parameter increases in wavelet transform. Second, smoothing allows the increasing of peaks significance in the wavelet spectrum. On the other hand, smoothing in average scale provides

some benefits. For instance, one is able to identify the fluctuations in power over range scale. Hence, the degrees of freedom of the points are increased and a relationship between significance levels and power is required for the analysis. The global time-averaged wavelet spectrum and scaled-averaged theoretical spectrum are given by:

$$\bar{W}^2(s) = (\frac{1}{N}) \sum_{n=0}^{N-1} |W_n(s)|^2 \quad (2.29)$$

$$\bar{P} = S_{average} \sum_{j=j_1}^{j_2} (P_j / s_j) \quad (2.30)$$

where s_j scale; P_j is the theoretical spectrum associated with s_j.; $S_{average}$ is the scale-averaged parameter.

Parameters for frequency content on seismic signals

There are some parameters that can be used to characterize the frequency content of earthquake signals (Rathje et al. 1998). These parameters are directly affected by earthquake magnitude and site conditions. The first parameter to study is the mean period (Tm).

$$T_m = \frac{\sum_i {C_i}^2 (1/f_i)}{\sum_i {C_i}^2} \; for \; 0.25 \; Hz \leq f_i \leq 20 \; Hz \quad (2.31)$$

Where C_i is the Fourier amplitude value of the entire accelerogram; the parameter f_i is related to the frequencies between 0.25 and 20 Hz from the Discrete Fourier transform (DFT). The parameter Tm is similar to the mean square frequency.

Another parameter to consider is the predominant period (Tp) which is defined as the period in which the maximum horizontal acceleration (MHA) occurs in an Acceleration Response Spectrum working with 5% damping.

In addition, the frequency parameter 'smoothed spectral predominant period' To is defined by means of the following expression.

$$T_O = \frac{\sum_{i=1}^{nPer} T_i * ln[S_a(T_i)] * H[S_a(T_i) - 1.20MHA]}{\sum_{i=1}^{nPer} ln[S_a(T_i)] * H[S_a(T_i) - 1.20MHA]} \quad (2.32)$$

Where nPer is the number of periods which were taken for the response spectrum; T_i is each discrete period in the response spectrum; MHA is the maximum horizontal acceleration; and H is the Heaviside function (H(x) = 0 for x<0 and H(x) =1 for x>0).

Another parameter to highlight is the average period (T_{avg}) which is similar to Tm, but the periods are equally spaced considering the horizontal axis. It is expressed as it follows.

$$T_{avg} = \frac{\sum_i T_i (S_a(T_i)/PGA)^2}{\sum_i (S_a(T_i)/PGA)^2} \; ; \; 0.05 \; \leq T_i \leq 4 \; s; \Delta T_i < 0.05 \; s \qquad (2.33)$$

Where PGA is the peak ground acceleration. Regarding the former expression, long periods, which are equally spaced, bring about dependent spectral accelerations because this feature depends on the natural frequency of a SDOF system (Rathje, Abrahamson, and Bray, 2004). The predominant period (Tp) has great variation for historical records. Conversely, the mean period (Tm) and smooth spectral predominant period (To) are considered to be more reliable; the mean period is preferred because it depends directly on the acceleration time history.

Histogram distribution

An adequate number of bins in histograms is important for informative purposes. There are many methods to obtain the number of bins for a histogram. In practice, it is recommended to use a number of bins approximately equal to the square root of the total of observations (Montgomery and Runger, 2015).

The histogram and normal fit distribution can be obtained by means of the Freedman-Diaconis rule which minimizes the difference between the theoretical probability distribution and the distribution obtained from analysis (Freedman et al. 2007). The optimal bins size is evaluated according to the following equation.

$$hbins = 2 * IQR(x(t))/(n^{1/3}) \quad (2.34)$$

Where hbins is the bins size; IQR (x(t)) is the interquartile range of the signal; n is the number of data points.

Then, the optimal number of histogram bins is obtained.

$$nbins = Range(x(t))/hbins \quad (2.35)$$

Cross correlation

The cross-correlation method is used to compare data sets considering time sequence (Cooper, G.H.R, 2017). The cross correlation of two continuous functions is denoted by the following:

$$(f * g)(\tau) = \int_{-\infty}^{+\infty} \bar{f}(t)g(t+\tau)dt = 0 \quad (2.36)$$

Where $\bar{f}(t)$ is the complex conjugate function of f(t); τ is the lag (shift).

For two time series, the linear correlation can be expressed as it follows:

$$r = \frac{\sum_i (X_i - \bar{X})(Y_i - \bar{Y})}{\sqrt{\sum_i (X_i - \bar{X})^2 \sum_i (Y_i - \bar{Y})^2}} ; \quad (2.37)$$

Where Xi and Yi are the time-series vectors; $\bar{X}$ and $\bar{Y}$ are the mean values for each time-series vector.

Root Mean Square Error (RMSE)

The Root Mean Square Error (RMSE) is one way to quantify the difference between and estimator and the observation. This parameter could be used to measure how well predicted values approximates real observations.

$$RMSE = \sum_{i=1}^{N} (F_i - O_i)^2/N \quad (2.38)$$

Where N is the number of pair observations; F_i is the forecast value; and O_i is each observation.

Goodness of fit for Peak Ground Acceleration (SPGA)

One way to compare synthetic acceleration and real ground motion is by means of evaluating how well the synthetic record predicts the peak ground acceleration of the real event (Anderson, 2004).

$$SPGA = S(A1, A2) = 10exp\left\{-\left(\frac{A1-A2}{\min(A1,A2)}\right)^2\right\} \quad (2.39)$$

Where A1 is the maximum absolute acceleration for the ground motion; A2 is the maximum absolute acceleration for the synthetic record. The factor 10 is used to have values within a comfortable range. Table 2.1 shows the possible scores and goodness-of fit interpretation for peak ground accelerations.

Table 2.1. Goodness-of-fit coefficient for PGA on seismic records (Reprinted from Anderson, 2004)

Score	Goodness-of-fit
10	Perfect
8-10	Excellent
6-8	Good
4-6	Fair fit
0-4	Poor

3 PREVIOUS EXPERIMENTAL STUDY

3.1 Full-scale adobe model description

A one-story full-scale adobe dwelling was built and subjected to seismic simulation at the Structures Laboratory at the Pontifical Catholic University of Peru (PUCP). The building was subjected to the 1970 Peruvian scaled acceleration earthquake signal; the shaking table platform allows a maximum displacement of 150 mm and 1.60 g acceleration; its maximum weight capacity is 160 kN. Cracks were induced in the adobe structure. Afterwards, the building was repaired by means of grout injection and reinforced with nylon ropes. A second seismic simulation was performed on the retrofitted model (Blondet et al. 2017). The model comprises 0.25 m thick adobe walls and has a 3 x 3 floor area. The material properties are specified according to Table 1.1 (Tarque et al. 2014). Figure 3.1 shows the adobe dwelling before the first shaking test (left) and after repair and reinforcement ready for a second seismic test (right).

Figure 3.1. One-story adobe building. Left. Building before first seismic test. Right. Damaged building (retrofitted) ready for second seismic test (Reprinted from Blondet et al. 2017).

The full-scale adobe model includes several building materials: concrete foundation ring, adobe masonry, timber roof and tiles. The earthquake signal direction was parallel to the lateral walls plane -left and right walls - (Figure 3.2).

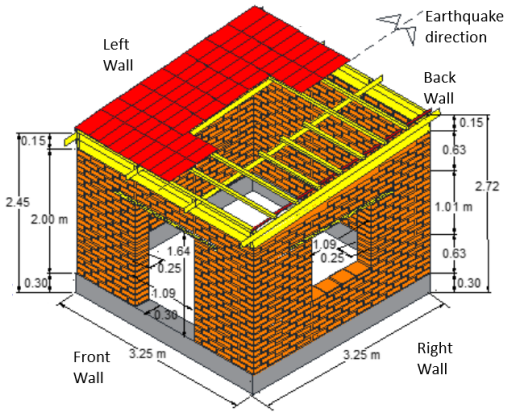

Figure 3.2. 3D Scheme for the one-story adobe building under seismic excitation.

3.2 Ground Acceleration

The ground acceleration signal is derived from the 31 May 1970 Peruvian earthquake (M = 7.75) component registered in Lima, Peru. Figure 3.3 shows the 30 second and scaled (0.3g) signal used for the model analysis; the signal was applied on the direction of the excitation (Blondet et al. 2004).

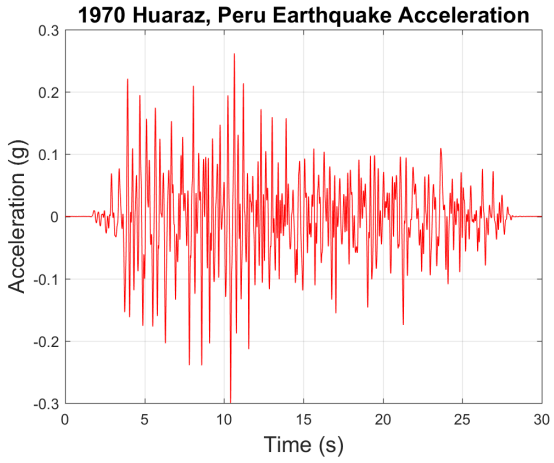

Figure 3.3. 1970 Peruvian earthquake ground acceleration signal (0.3 g scaled).

The peak ground acceleration (PGA) of the 1970 Peruvian was 0.10 g (registered in Lima, 240 miles from epicenter) and lasted around 45 seconds (Saragoni et al. 2014). Table 3.1 shows the Moment Magnitude (Mw) and PGA (maximum recorded) for some common earthquakes compared with the 1970 Peruvian event.

Table 3.1. The 1970 Peruvian earthquake compared with other seismic events

Earthquake	Date	Magnitude (Mw)	Maximum PGA (g)
El Centro	1940	6.90	0.30
Huaraz, Peru	1970	7.75	0.10
Kobe	1995	6.90	0.80
Chile	2010	8.80	0.78

The Fast Fourier Transform (FFT) MATLAB command was used to evaluate the Fourier Transformation of the earthquake signal. The transformation considered a sample frequency fs = 200 Hz (dt = 0.005 s) for the FFT command (Figure 3.4).

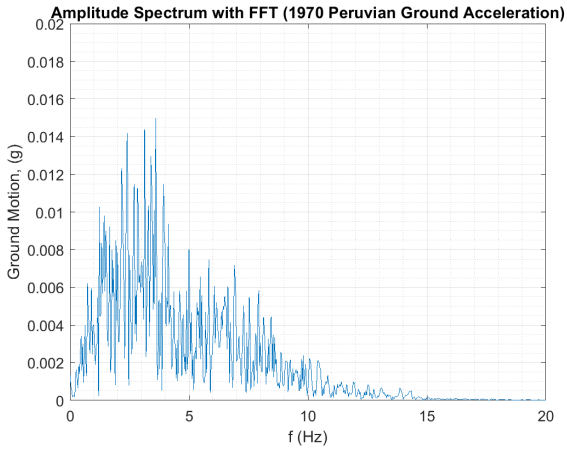

Figure 3.4. Fourier Amplitude Spectrum of the 1970 Peruvian earthquake (0.3g scaled) with sampling frequency fs = 200 Hz. Fast Fourier Transformation (FFT)

The dominant frequencies are located around 2, 3 and 4 Hz approximately. The peak value is related to the 3.5 Hz frequency content.

3.3 Shaking table tests

A real earthquake presents six directions (three rotations and three translation displacements). Nevertheless, the shaking table at the Catholic University of Peru (PUCP) has one direction movement for the simulations. Therefore, the energy in the shaking test is different from what could be expected in a real earthquake.

Hence, the PUCP's shaking table displacement (phase) is associated with an earthquake class as shown in Table 3.2 (Bossio, 2010).

Table 3.2. Test phases at PUCP's shaking table

Phase	Displacement	Earthquake
ID	Maximum (mm)	Intensity (level)
Phase 1	30	Minor
Phase 2*	60	Light
Phase 3	90	Moderate
Phase 4	130	Severe

*Used for this research project.

The full-scale adobe model was subjected to two shaking tests. The first test was performed on the original undamaged model (phases 1 and 2). After repair and retrofitting, the adobe dwelling was subjected to a second shaking test (phases 1, 2, 3 and 4 twice). Before each shaking test, a free vibration movement was performed with a 1.50 mm rectangular pulse signal. The phase 2 data content was used for the present research analysis.

3.4 Instrumentation

The two seismic simulations considered the same instrument configurations: 10 accelerometers and 8 linear variable displacement transducers (LVDT). The acceleration and displacement results for the shaking table were also measured (A0 and D0) to obtain relative displacements and accelerations. Figure 3.5 shows the plan and 3D view of the instrumentation.

The devices located on the top of the model are of particular interest due to their magnitude. Accelerometers 1 and 2 are located on the right and left top wall, respectively on planes parallel to the shaking direction. Accelerometers 3 and 4 are located on the front and back wall, respectively of the adobe structure and are placed on planes perpendicular to shaking

direction. Hence, Accelerometer 0 is located on the shaking table platform and it is used to confirm the accuracy of the excitation.

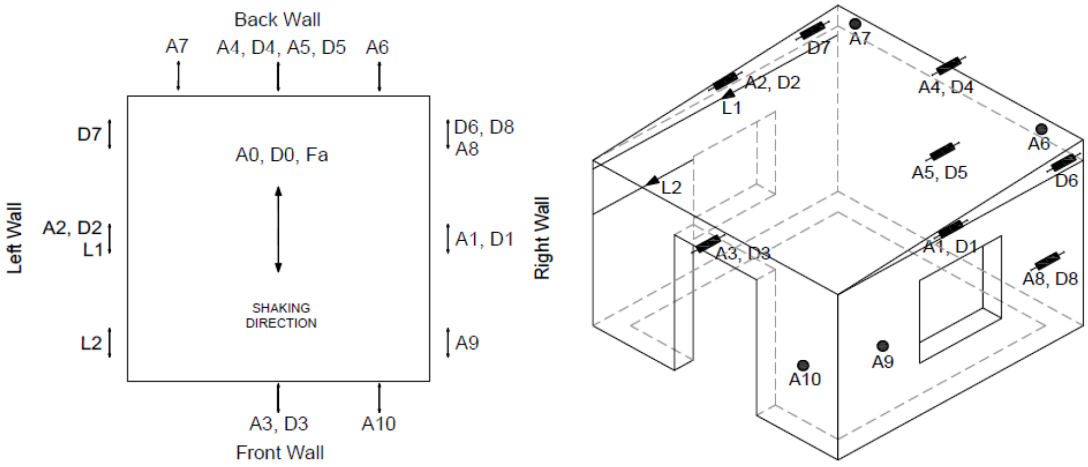

Figure 3.5. Instrumentation on full-scale adobe model.

3.5 Interpretation of the experimental data

The two seismic simulations provided data for phase 1 (D = 30 mm) and phase 2 (D = 60 mm). Statistical analysis was performed for the experimental accelerometers signals regarding phase 2. Parameters such as standard deviation, skewness and kurtosis were obtained. Accelerometers 1 and 2, located at the top of the building and parallel to shaking direction, provide high acceleration values. Provided that they also offer high relative displacement values after seismic simulation, these signals give relevant information for analysis.

3.5.1 Response of the undamaged structure

Table 3.3 shows the statistics for the first seismic test on the undamaged full-scale adobe model (Phase 2 with Displacement = 60 mm).

Table 3.3. Statistics on accelerometers response after first seismic test (phase 2)

Accelerometer	Acceleration		Statistics		
ID	Maximum (g)	Minimum (g)	Standard Dev. (g)	Skewness	Kurtosis Coeff-3
A0	0.532	-0.639	0.144	-0.190	1.853
A1	1.009	-1.206	0.344	-0.390	0.864
A2	0.954	-0.873	0.256	-0.061	1.287
A3	1.347	-1.778	0.358	-0.197	1.232
A4	1.356	-0.865	0.295	0.668	1.255
A5	0.838	-0.668	0.193	0.353	1.501
A6	1.089	-0.750	0.271	0.447	0.920
A7	1.035	-0.655	0.226	0.487	1.395
A8	0.669	-0.551	0.178	0.224	1.175
A9	0.603	-0.927	0.226	-0.748	1.516
A10	0.547	-0.686	0.169	-0.419	1.602

Negative skewness stands for long left tails while positive skewness represents long right tails. A0 (control accelerometer) presents a small skewness value. This issue is due to the signal and shaking direction.

The kurtosis for a normal standard distribution is 3; small kurtosis represents light-tailed distribution while positive kurtosis values (higher than 4) stands for somewhat heavy-tailed distribution. The former table clearly shows heavy-tailed distribution especially for accelerometers A0. A1 and A2, located at the top of the building and parallel to shaking direction, present heavy tails.

3.5.2 Response of the retrofitted structure

Another statistical analysis is provided for the second seismic test for the cracked-and-repaired full-scale adobe model (Phase 2 with Displacement = 60 mm).

Table 3.4. Statistics on accelerometers response after second seismic test (phase 2)

Accelerometer	Acceleration		Statistics		
ID	Maximum (g)	Minimum (g)	Standard Dev. (g)	Skewness	Kurtosis Coeff-3
A0	0.509	-0.711	0.140	-0.264	2.054
A1	1.145	-1.165	0.350	-0.217	1.323
A2	0.653	-0.706	0.165	0.227	1.829
A3	1.619	-2.250	0.486	-0.409	1.342
A4	1.223	-1.349	0.351	0.051	0.932
A5	0.699	-0.882	0.238	-0.453	1.053
A6	1.199	-0.811	0.297	0.548	1.189
A7	0.714	-0.709	0.200	0.048	1.138
A8	0.758	-0.686	0.197	0.521	1.320
A9	0.511	-0.737	0.168	-0.194	1.285
A10	0.558	-0.721	0.172	-0.118	1.383

A0 (control accelerometer) presents a relative bigger skewness (asymmetry) value on the retrofitted model compared to the undamaged structure. Damage in the structure could have contributed to the difference. A1 presents smaller skewness in the retrofitted model while A2 presents a bigger one compared with the original model. The interaction among adobe blocks on the second test (retrofitted model) could have contributed towards this effect.

3.5.3 Comparison between original and retrofitted experimental response

To compare the similarity of two discrete time series signals, the cross-correlation method is used. This method is applied to the acceleration response for the undamaged model and the one related to the retrofitted model; both responses are studied for phase 2 with displacement D = 60 mm. Table 3.5 shows the results for the cross-correlation considering lag 0 seconds for the two signals, and response on retrofitted model shifted 5 seconds from the undamaged model.

Table 3.5. Cross-correlation for acceleration on original and retrofitted model

Accelerometer	Cross correlation	
ID	At lag 0 s	At lag 5 s
A0	0.91	0.80
A1	0.99	0.82
A2	-0.97	-0.80
A3	0.99	0.83
A4	0.99	0.82
A5	-0.99	-0.83
A6	0.98	0.83
A7	0.99	0.83
A8	0.99	0.83
A9	0.99	0.83
A10	-0.99	-0.83

High cross correlation stands for most similarity in signals (approximation to 1 or -1). Accelerometers 1 and 2 (parallel to shaking direction) have similar correlation values at lag 0 s (0.99 and -0.97; the signals after the first and second seismic test are somewhat similar. The difference could have been brought about because of the damage and therefore retrofitted behavior of the adobe house.

4 ABAQUS MODEL OF A ONE-STORY ADOBE STRUCTURE

ABAQUS software allows users to analyze and model different types of structures. ABAQUS work with modules which define geometry, material properties, mesh, monitoring, and results (ABAQUS, 2018). For instance, this software provides the characterization of mechanical properties of different materials such as adobe. In fact, its modulus of elasticity, weight per volume and Poisson ratio can be defined.

The full-scale adobe dwelling was modeled by means of ABAQUS; the software brings about several response results. For example, time-history displacements, accelerations and modal parameters can be obtained. Time-domain plots will be of interest for the Fourier and Wavelet transform methods.

4.1 First shaking test: original structure

The first shaking test was performed on the full-scale original undamaged model. ABAQUS was used to model the different materials and properties in the adobe dwelling. For instance, the concrete ring, adobe walls, and timber roof were represented (Figure 4.1).

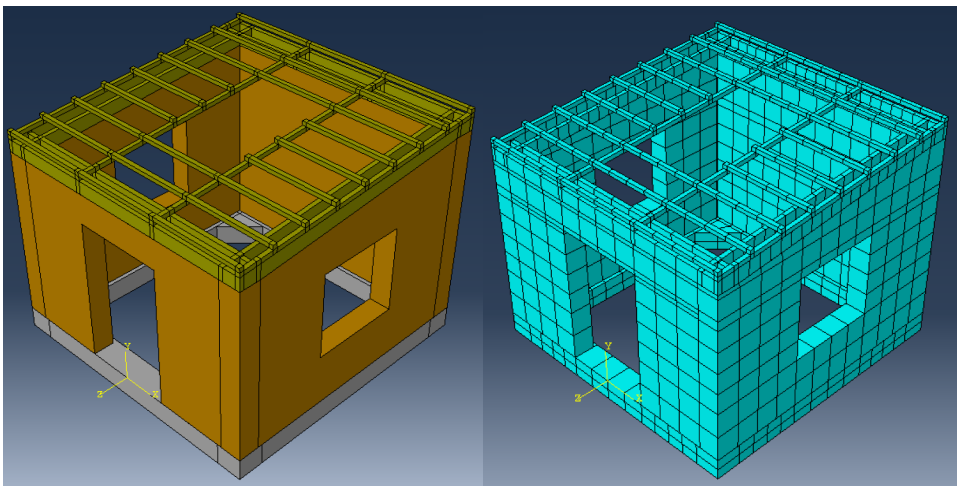

Figure 4.1.ABAQUS Full-scale original adobe model under seismic excitation. Left. Assembly model. Right. Mesh representation.

Figure 4.2 shows the details regarding the left and back wall. Concrete ring, adobe walls and roof are joined by means of a TIE constraint which works well with dissimilar regions.

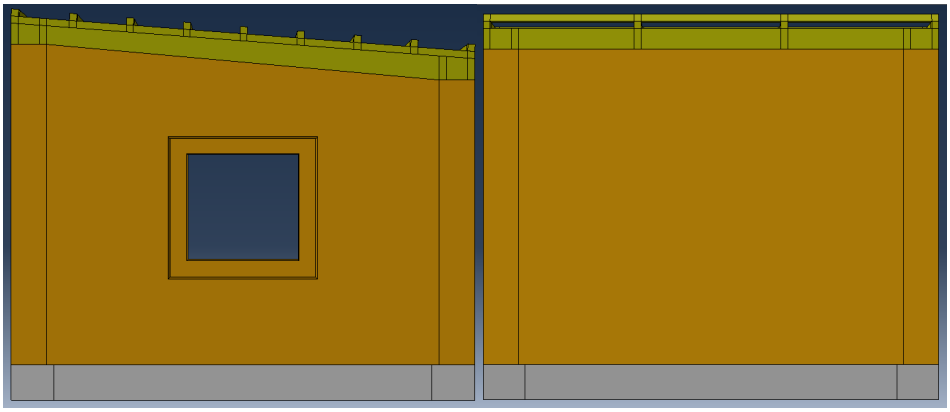

Figure 4.2. ABAQUS Full-scale undamaged adobe model under seismic excitation: Left wall and back wall representation.

Openings such as the front wall and lateral windows are modeled. Hence, the timber collar beam and joists were represented; the rectangular central opening at the top of the roof allows the transportation from construction site to shaking table (Figure 4.3).

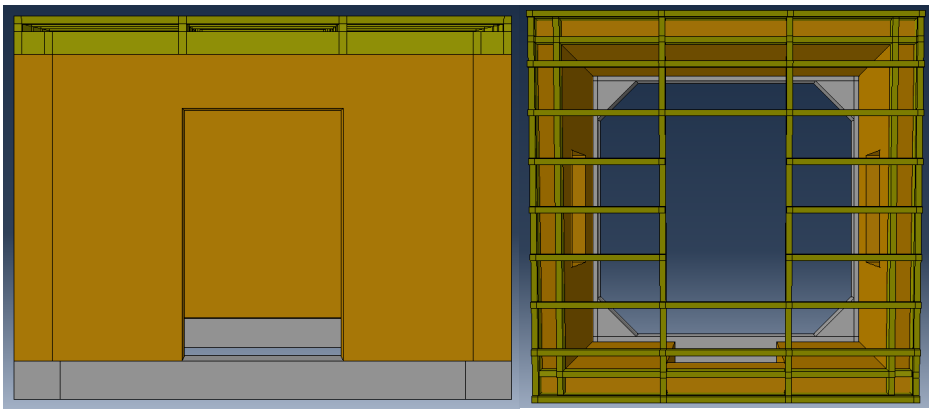

Figure 4.3. ABAQUS Full-scale original adobe model under seismic excitation: Front Wall and timber roof representation.

4.2 Second shaking test: retrofitted structure

After the first seismic simulation, the adobe dwelling presented cracked adobe blocks. Then, the cracks were repaired by means of liquid mud and walls were reinforced with horizontal and vertical nylon strings. Next, the repaired-and-retrofitted adobe model was subjected to a second seismic test. Adobe blocks and horizontal nylon strings were modeled (Figure 4.4).

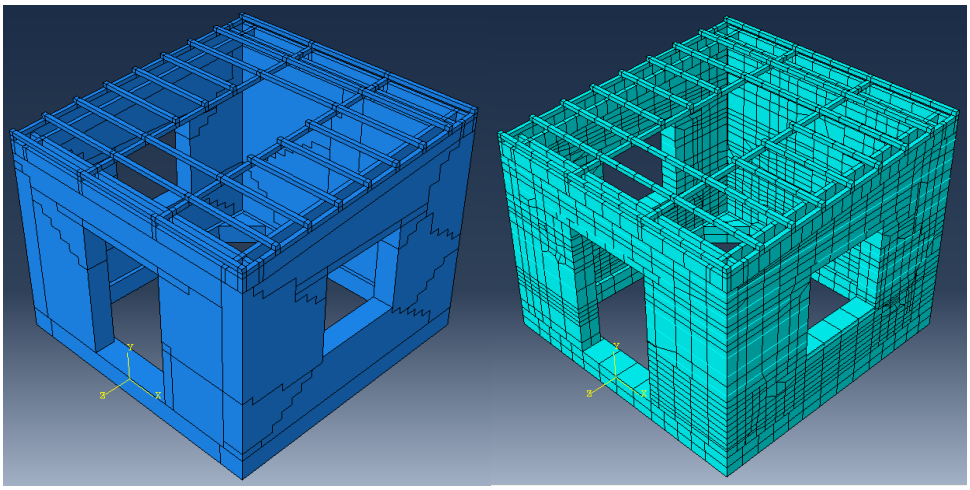

Figure 4.4. ABAQUS Full-scale cracked adobe model. Left. Assembly model. Right. Mesh representation.

After the first seismic test, 14 adobe blocks detached from the main structure. For instance, two adobe blocks located both on the front and left wall are shown (Figure 4.5).

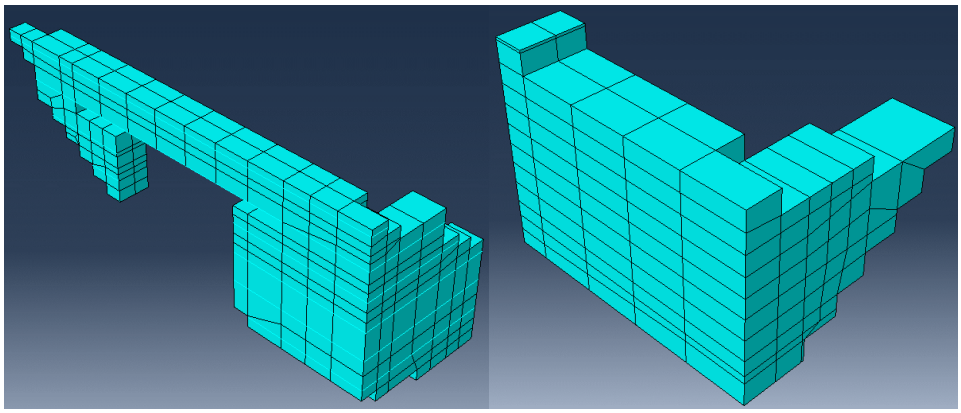

Figure 4.5. Adobe blocks on ABAQUS adobe cracked building.

Horizontal nylon strings were modeled by means of stringer property on each adobe block. For analysis, the ¼" string has an elasticity modulus (E) = 60 MPa (Blondet et al. 2017). Figure 4.6 shows the details regarding the left and back wall. Vertical lines represent cut planes on ABAQUS adobe blocks. Concrete ring, adobe walls and roof are joined by means of TIE constraint which works well with dissimilar surfaces.

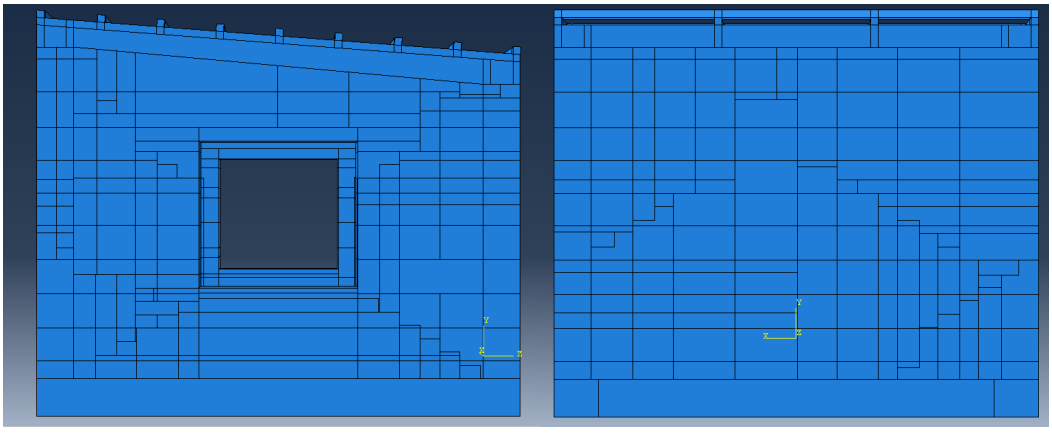

Figure 4.6. ABAQUS Full-scale retrofitted adobe model: Left wall and back wall representation.

4.3 Experimental and predicted acceleration

ABAQUS software provides time history responses for both the first and second shaking tests. For comparison purposes, phase 2 (D = 60 mm) for both shaking tests was studied for accelerometers 1 and 2; these accelerometers are located on the top of the right and left wall, respectively. Then, plots such as the Fourier Amplitude and Power Spectral Density were obtained. Comparison between experimental and numerical data is presented.

4.3.1 Accelerometer 1

After the two shaking tests (phase 2 with D = 60 mm), the accelerometer 1 registered similar time-history responses for both the experiment and numerical data (Figure 4.7 and Figure 4.8). The peak acceleration response is around 1g for the experiment data and the numerical simulations.

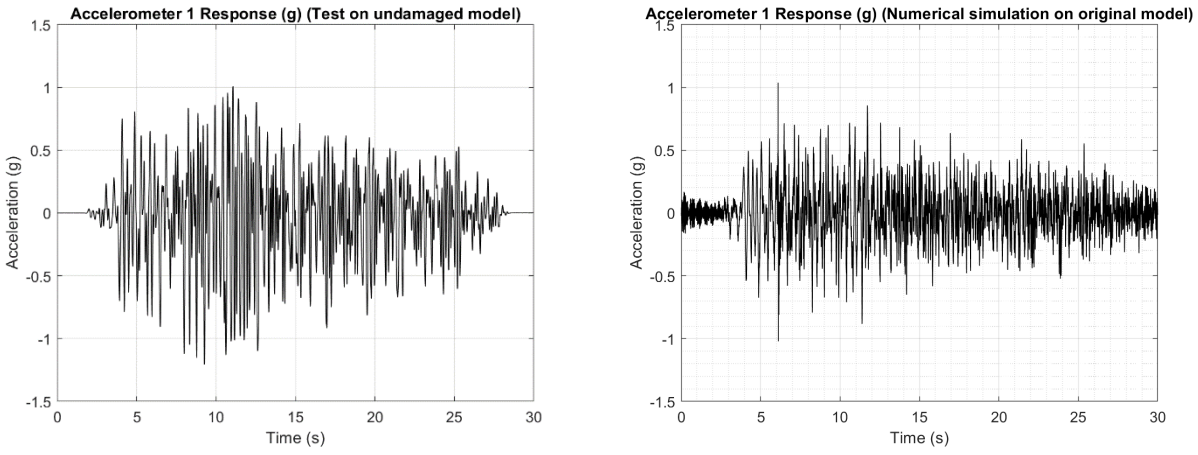

Figure 4.7. Accelerometer 1 response on original model (test and numerical model). Left: Experiment test. Right: ABAQUS numerical model.

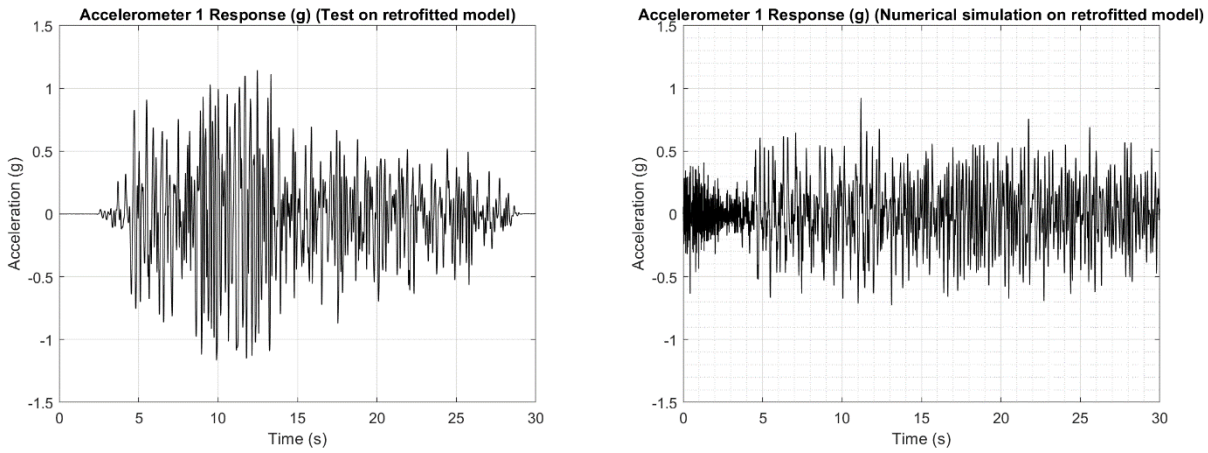

Figure 4.8. Accelerometer 1 response on retrofitted model (test and numerical model). Left: Experiment test. Right: ABAQUS numerical model.

To compare the similarity of two discrete time series signals, the cross-correlation method can be used. This method is applied to the acceleration response provided by the experiment and the ABAQUS model; both responses are studied for phase 2 with displacement D = 60 mm. Table 4.1 shows the results for the cross-correlation considering lag 0 and shifted 5 seconds for the response in accelerometer 1 for the undamaged and retrofitted model. The Root Mean Square Error (RMSE) is also presented.

Table 4.1. Comparative analysis for acceleration 1 on test and ABAQUS

Accelerometer1	Cross-correlation		RMSE	SPGA
Building	At lag 0 s	At lag 5 s	Abaqus-test	Parameter
Original	0.98	0.83	0.61	9.87
Retrofitted	-0.98	-0.82	0.52	9.36

High cross correlation stands for most similarity in signals. Accelerometer 1 (parallel to shaking direction) shows high correlation (0.98) for the original and retrofitted model in

ABAQUS. Hence, the cross-correlation value at lag 5 s decreases for the models. The RMSE for the undamaged model is bigger than the retrofitted model. The SPGA coefficient represents an excellent fit (8 – 10) por the predicted Peak Ground Acceleration (PGA) in the numerical simulations.

In addition, the Fast Fourier Transformation provides the Amplitude Spectrum of the acceleration signals for both shaking tests. The FFT consider dt = 0.005 s (f = 200 Hz) for the real experiment and for the numerical simulations. (Figure 4.9 and Figure 4.10).

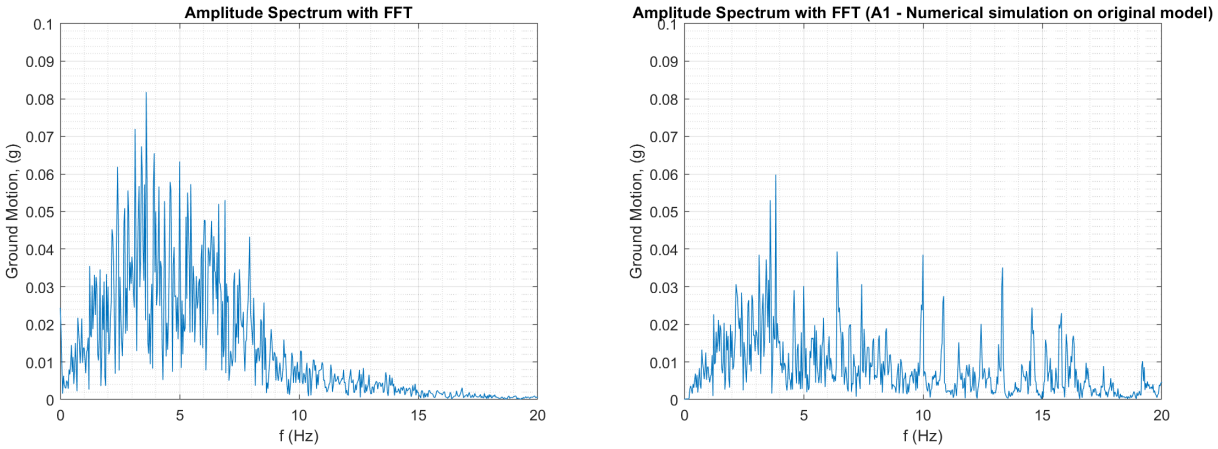

Figure 4.9. Fourier Amplitude Spectrum for Accelerometer 1 (original model). Left: Experiment (phase 2, D = 60 mm). Right: ABAQUS simulation (phase 2, D = 60 mm).

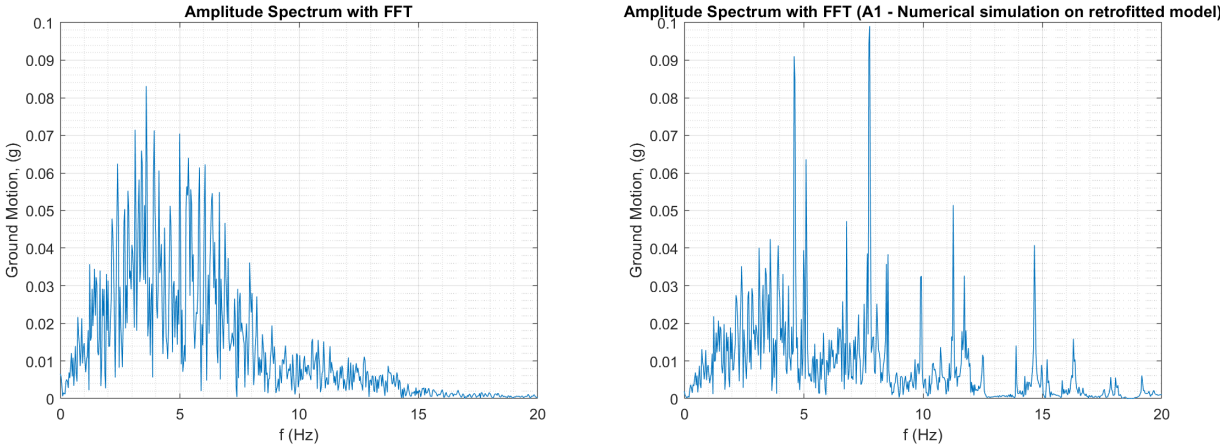

Figure 4.10. Fourier Amplitude Spectrum for Accelerometer 1 (retrofitted model). Left: Experiment (phase 2, D = 60 mm). Right: ABAQUS simulation (phase 2, D = 60 mm).

The FFT transform shows that there is a peak around 3.5 Hz for the experiments in the original models; this value is similar to the one obtained from ground motion signal (3.5 Hz). On the other hand, the transform plots are similar for both ABAQUS simulations. Peaks are detected for 4Hz (both simulations). Hence, Power Spectral Densities (PSD) curves for both tests are shown (Figure 4.11 and Figure 4.12).

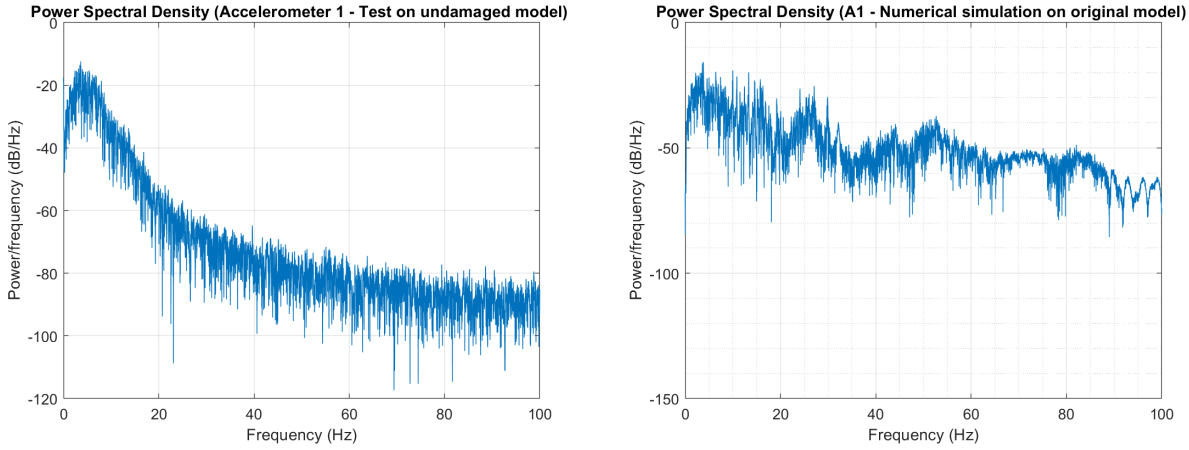

Figure 4.11. Power Spectral Density (PSD) for accelerometer 1 (original model). Left: Experiment (phase 2, D = 60 mm). Right: ABAQUS simulation (phase 2, D = 60 mm).

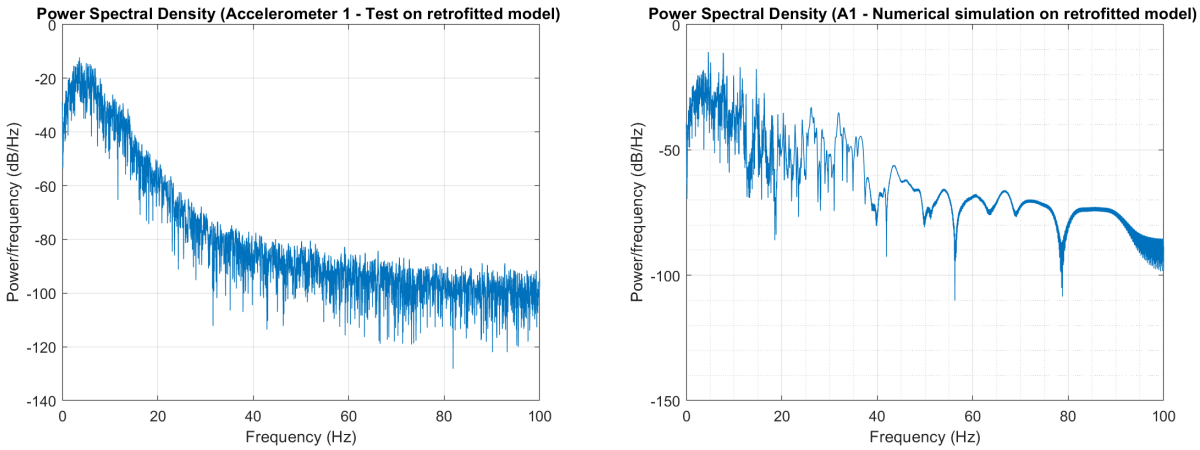

Figure 4.12. Power Spectral Density (PSD) for accelerometer 1 (retrofitted model). Left: Experiment (phase 2, D = 60 mm). Right: ABAQUS simulation (phase 2, D = 60 mm).

The experiments on both the original and retrofitted adobe house bring about similar plots for the power spectral density; a maximum power/frequency 120 db/Hz is detected for the real tests. Regarding numerical simulation, the retrofit technique brings a peak around 90 db/Hz.

4.3.2 Accelerometer 2

After the two shaking tests (phase 2 with D = 60 mm), the accelerometer 2 registered similar time-history responses for test data and numerical simulation (Figure 4.13 and Figure 4.14). The peak acceleration response is around 1g for the undamaged model. For the retrofitted adobe house, it approximates 0.6 g and 1.2 g for the test and numerical simulation, respectively.

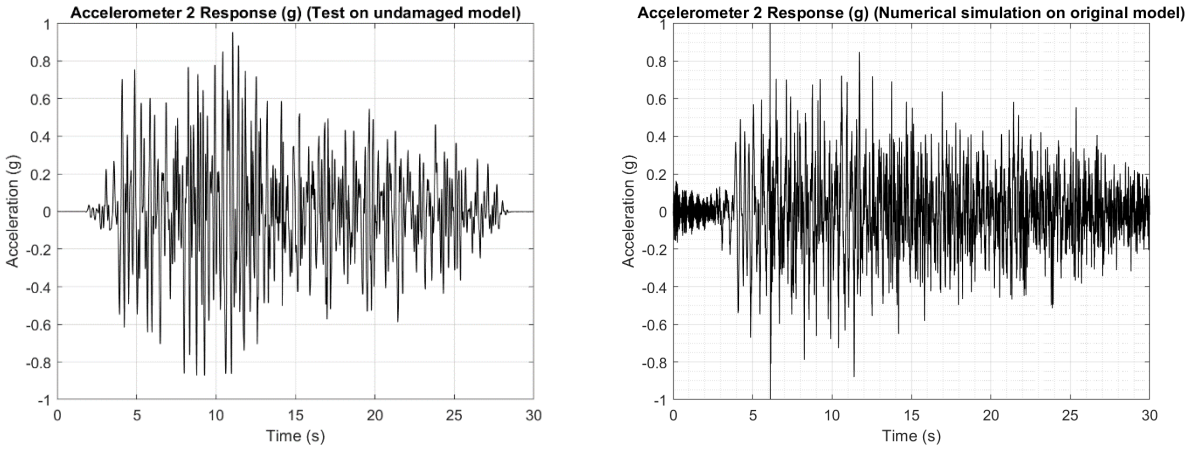

Figure 4.13. Accelerometer 2 response on undamaged model (test and numerical model). Left: Experiment test. Right: ABAQUS numerical model.

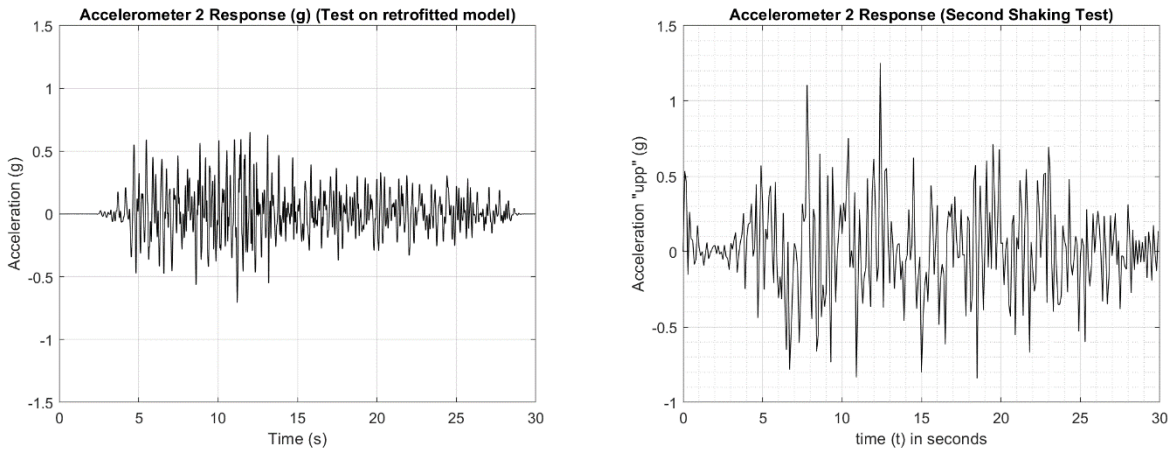

Figure 4.14. Accelerometer 2 response on retrofitted model (test and numerical model). Left: Experiment test. Right: ABAQUS numerical model.

The similarity of the discrete time signals for both cases (original and retrofitted model) is evaluated by means of the cross-correlation method. This method is applied comparing the acceleration response provided by the experiment and the ABAQUS model; both responses are studied for phase 2 with displacement D = 60 mm. Table 4.2 shows the results for the cross-correlation considering lag 0 seconds and lag 5 seconds (retrofitted model shifted from the original one) for the response in accelerometer 2. The Root Mean Square Error (RMSE) is also presented.

Table 4.2. Comparative analysis for acceleration 2 on test and ABAQUS

Accelerometer1	Cross correlation		RMSE	SPGA
Building	At lag 0 s	At lag 5 s	Abaqus-test	Parameter
Original	0.98	0.82	0.55	9.20
Retrofitted	0.96	0.83	0.70	4.12

High cross correlation stands for most similarity in signals. Accelerometer 2 (parallel to shaking direction) shows high correlation for the original and retrofitted model in ABAQUS. At lag 5 s, the correlation is similar in both conditions (0.83); this feature is similar to the ones observed in accelerometer 1. Regarding the RMSE, the original model provided a lower value compared to the retrofitted one. The SPGA coefficient provides an excellent fit (8-10) for the original model and a fair fit (4 – 6) for the retrofitted model regarding the predicted PGA in the numerical simulations.

Fast Fourier Transformation provides the Amplitude Spectrum of the acceleration signals for both shaking tests. The FFT considers dt = 0.005 s (f = 200 Hz) for the real experiment and the numerical simulation. (Figure 4.15 and Figure 4.16).

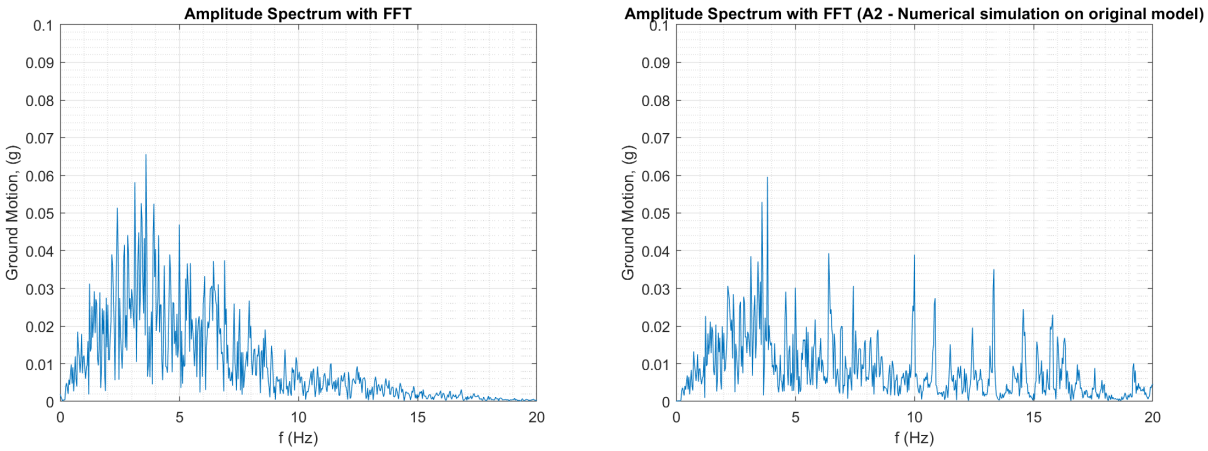

Figure 4.15. Fourier Amplitude Spectrum for Accelerometer 2 (original model). Left: Experiment (phase 2, D = 60 mm). Right: ABAQUS simulation (phase 2, D = 60 mm).

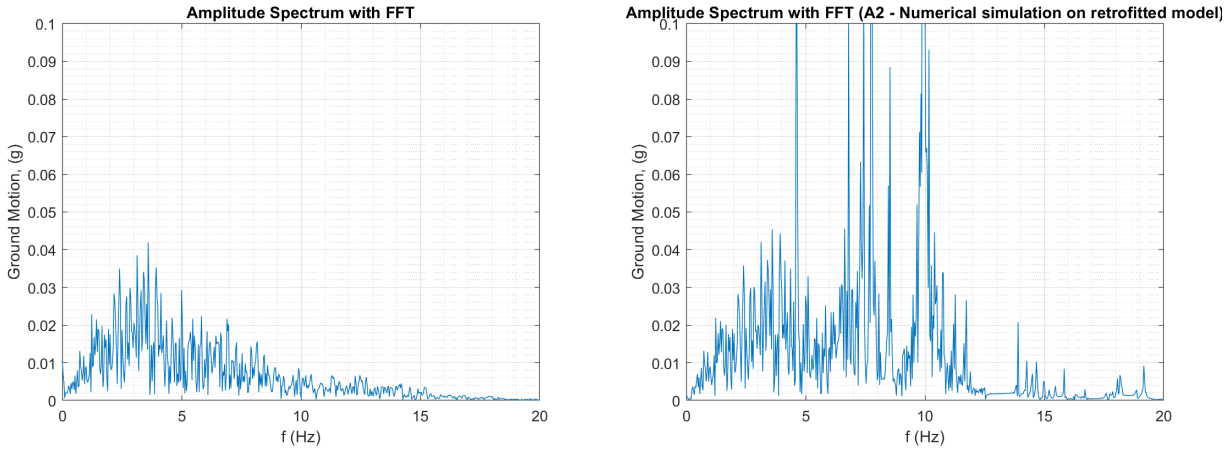

Figure 4.16. Fourier Amplitude Spectrum for Accelerometer 2 (retrofitted model). Left: Experiment (phase 2, D = 60 mm). Right: ABAQUS simulation (phase 2, D = 60 mm).

The FFT transform shows that there is a peak around 3.5 Hz for the experiments in the original and retrofitted models; the ground motion signal shows a similar behavior. On the other hand, the transform plots are not similar for the ABAQUS simulations. Peaks are detected for 3.5 and 5 Hz (original and retrofitted model, respectively). Hence, Power Spectral Densities (PSD) curves for both tests are shown (Figure 4.17 and Figure 4.18).

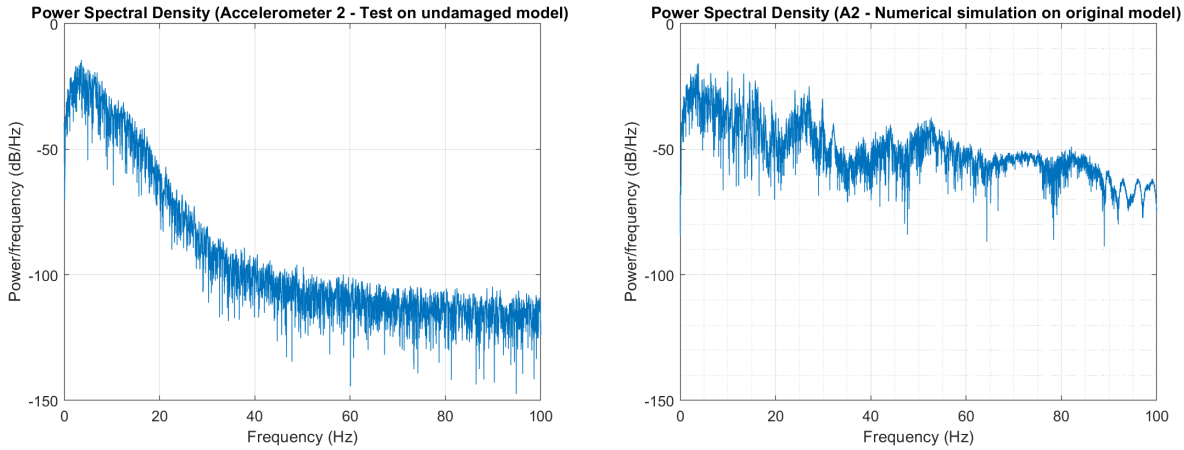

Figure 4.17. Power Spectral Density (PSD) for accelerometer 2 (original model). Left: Experiment (phase 2, D = 60 mm). Right: ABAQUS simulation (phase 2, D = 60 mm).

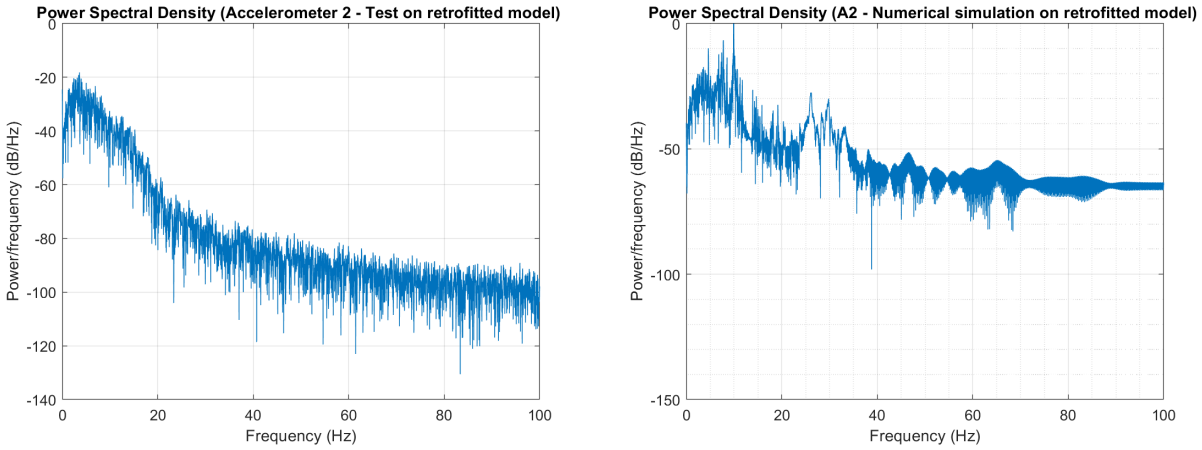

Figure 4.18. Power Spectral Density (PSD) for accelerometer 2 (retrofitted model). Left: Experiment (phase 2, D = 60 mm). Right: ABAQUS simulation (phase 2, D = 60 mm).

The experiments on both the original and retrofitted adobe house bring about similar plots for the power spectral density; a maximum power/frequency 120 db/Hz is detected for the real test (original and retrofitted structure) and around 70 db/Hz for the ABAQUS models.

4.4 Natural Frequency estimation

ABAQUS software brings about the natural frequency modes for the whole original undamaged one-story adobe model by means of frequency (eigenvalue) extraction. The eigenvalue extraction is a linear procedure which gives the natural frequencies and then the corresponding modes. The first six natural frequencies for the undamaged model are obtained (Table 4.3).

Table 4.3. Estimated frequencies for undamaged adobe model

Mode	Frequency
	(Hz)
First	2.44
Second	3.27
Third	3.44
Fourth	3.68
Fifth	3.83
Sixth	4.17

The dominant frequencies related to the ground acceleration input are approximately 2, 3 and 4 Hz. The first modes do provide resonance effect in the adobe model; therefore, damages are likely to be amplified. First mode is associated with big bending effects on the back wall. The second and third modes show strong bending effects on the left and right walls (lateral walls) close to the central opening; high bending effects are appreciated close to the back wall. Hence, the fourth and fifth modes bring about high displacements in the central part of the front wall. Regarding the sixth mode, displacements in both the front and back wall are notorious (Figure 4.19).

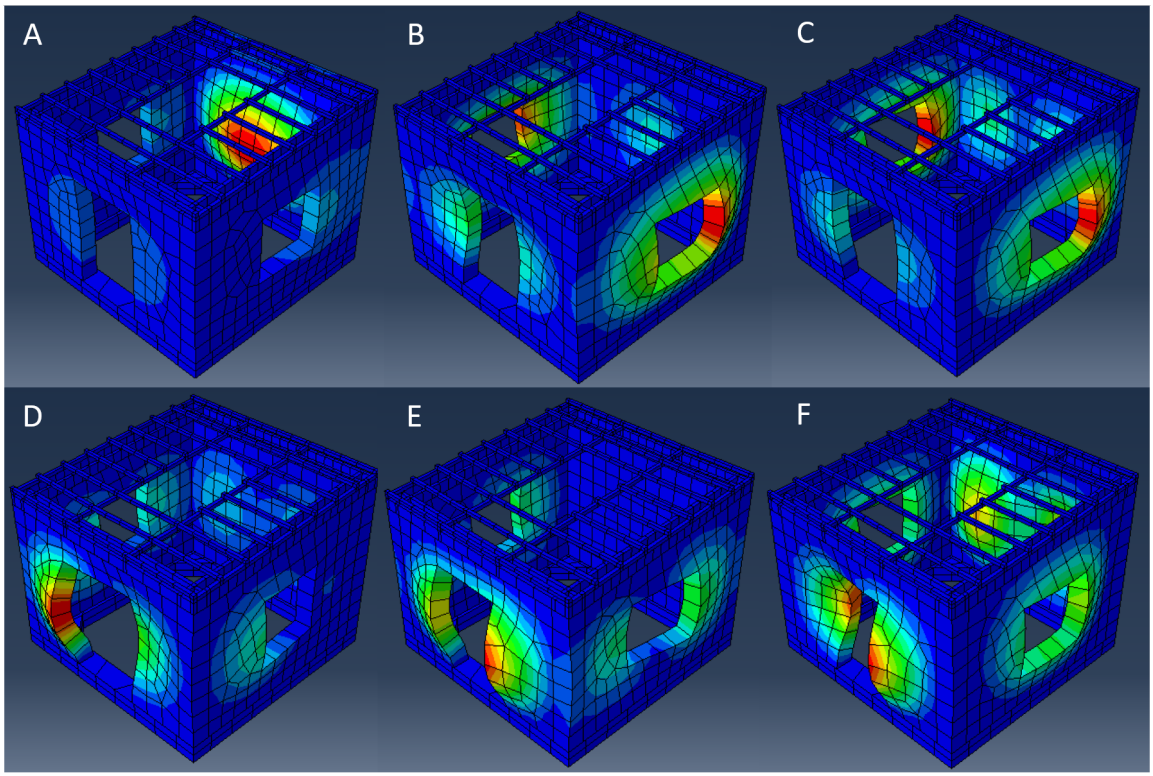

Figure 4.19. Estimation of the first six modes for the undamaged one–story adobe building. A) 2.44 Hz B) 3.27 Hz C) 3.44 Hz D) 3.68 Hz E) 3.83 Hz F) 4.17 Hz.

ABAQUS also provides the natural frequency modes for the whole retrofitted one-story adobe model by means of frequency (eigenvalue) extraction. The first six natural frequencies for the are shown (Table 4.4).

Table 4.4. Estimated frequencies for retrofitted adobe model

Mode	Frequency
	(Hz)
First	4.54
Second	4.81
Third	5.40
Fourth	6.40
Fifth	6.84
Sixth	7.04

The dominant frequencies related to the ground acceleration input are approximately 2, 3 and 4 Hz. In the retrofitted adobe model, the first two modes do provide resonance effect in the adobe model. First mode is associated with bending effects on the left wall. The second and third modes show strong bending effects on the right wall (close to the central window) and in the back wall. Hence, the fourth mode depicts bending in the left and right (lateral walls); the fifth mode shows displacement in the base of the front wall. Regarding the sixth mode, bending in two opposite corners (close to the central window) is notorious (Figure 4.20).

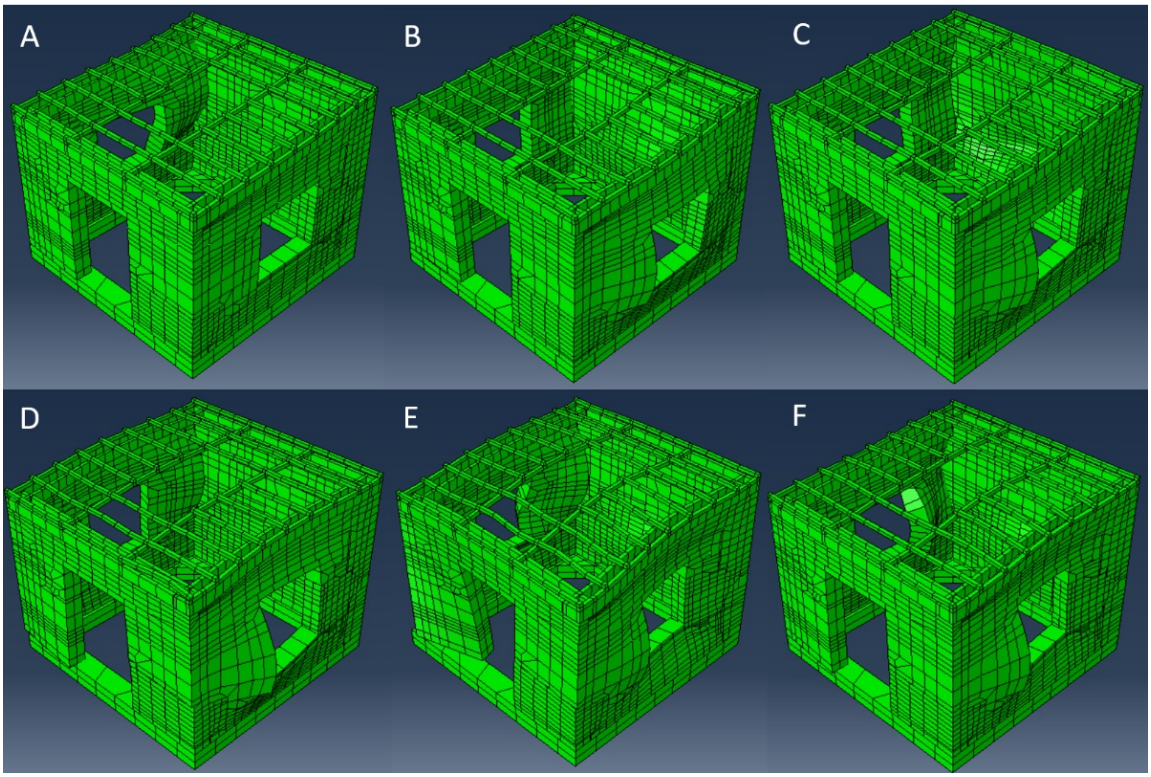

Figure 4.20. Estimation of the first six modes for the retrofitted one–story adobe building. A) 4.54 Hz B) 4.81 Hz C) 5.40 Hz D) 6.40 Hz E) 6.84 Hz F) 7.04 Hz.

5 STATISTICAL ANALYSIS

5.1 Ground acceleration

The two shaking tests consider phase 1 (D = 30 mm) and phase 2 (D =60 mm). Regarding phase 2, the 1970 (0.6 g scaled) Peruvian ground acceleration was analyzed according to formulas 3.1 and 3.2 to obtain the optimal bin size (0.1213 m/s^2), and optimal number of bins (91), respectively. For practical purposes, the analysis considered 0.10 m/s^2 for bin size and therefore 111 number of bins.

The probability distribution function (pdf) and cumulative distribution function (cdf) were obtained by means of MATLAB script. The basic idea for continuous data is that, for very large samples, the histogram distribution approximates a continuous function (pdf) associated with a random variable (Cline, 2017). Figure 5.1 shows the histogram (density distribution) and normal fit for the 0.6g scaled ground acceleration signal. The distribution shows symmetry and light tails with the optimal number of bins. However, zero acceleration provides high density distribution.

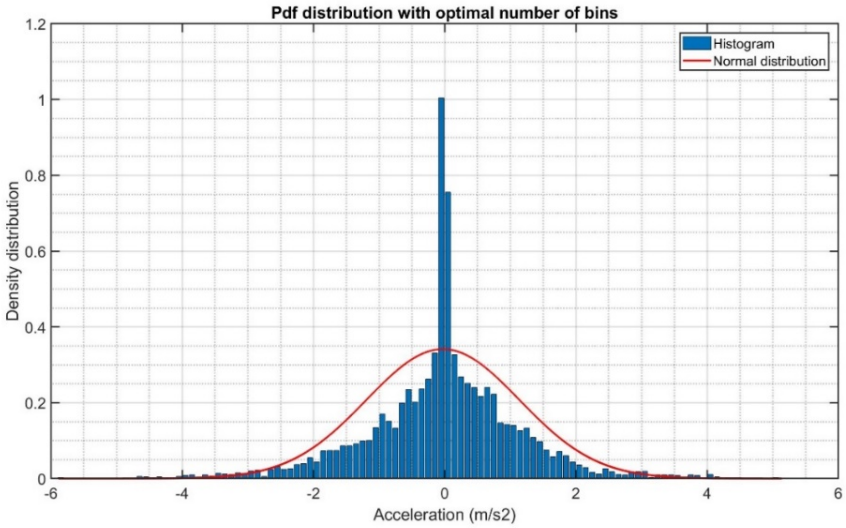

Figure 5.1. Density distribution and normal fit for the 0.6g scaled ground acceleration.

The histogram distribution brings about several statistics. Table 6.1 shows the results for the 0.60g scaled acceleration signal.

Table 5.1. Statistics for the 0.60 g scaled ground acceleration signal

Acceleration		Statistics		
Maximum (g)	Minimum (g)	Standard Dev. (g)	Skewness	Kurtosis
0.524	-0.600	0.119	-0.214	-2.432

The scaled signal shows a kurtosis value close to a Gaussian distribution (kurtosis = 3). In fact, negative kurtosis depicts light-tailed distribution as it is shown in the histogram.

As acceleration values increases, the cumulative probability enhances. The cumulative distribution function (cdf) is obtained for the 0.6g ground acceleration signal (Figure 5.2).

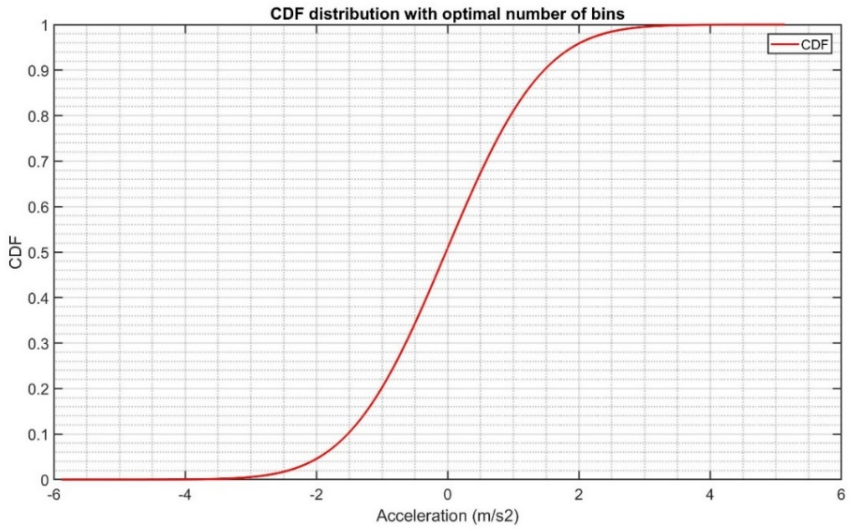

Figure 5.2. Cumulative Distribution Function (cdf) for the 0.6g scaled ground acceleration.

5.2 First shaking test: original structure

The pdf and cdf distribution were obtained for accelerometers 1 and 2 for both the ABAQUS and experiment data (second phase D = 60 mm). Figure 5.3 shows that the ABAQUS model is relatively close to the real data regarding accelerometer 1; the pdf shows symmetry in both curves and the cdf depicts close approximation. The difference between the experiment and the model can be brought about due to the assumptions in the numerical model and the particular instrumentation.

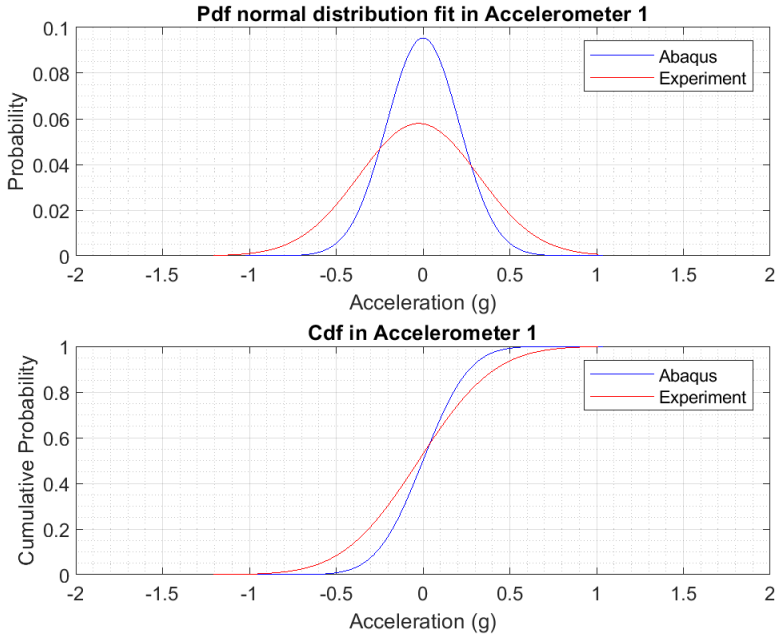

Figure 5.3. Shaking test on original structure: pdf and cdf for accelerometer 1 (ABAQUS and experimental data).

Regarding accelerometer 2, the numerical model provides similar values related to experimental data for both the pdf and cdf (Figure 5.4). The probability function depicts values similar to accelerometer 1 (ABAQUS model).

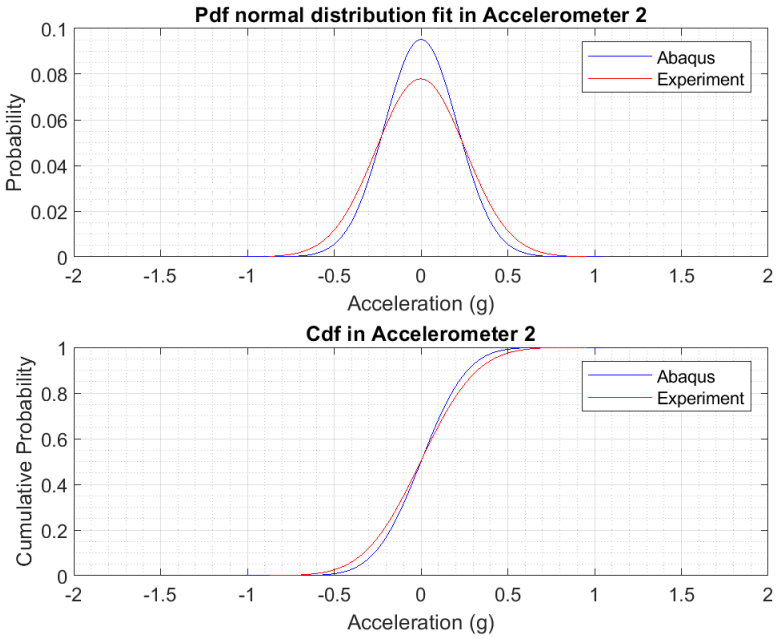

Figure 5.4. Shaking test on original structure: pdf and cdf for accelerometer 2 (ABAQUS and experimental data).

Regarding statistics, the accelerometers 1 and 2 provided similar results compared to the ones obtained from the real experiment (Table 5.2).

Table 5.2. Statistics on accelerometers after seismic test on original model (phase 2)

Accelerometer	Acceleration		Statistics		
ID	Maximum (g)	Minimum (g)	Standard Dev. (g)	Skewness	Kurtosis Coeff. -3
A1 – Test	1.009	-1.206	0.344	-0.390	0.864
A2 – Test	0.954	-0.873	0.256	-0.061	1.287
A1 - Abaqus	1.039	-1.022	0.209	0.043	1.090
A2 - Abaqus	1.035	-1.032	0.210	0.041	1.081

The ABAQUS model brings about a relative good approximation for the real experiment. The Kurtosis coefficient depicts heavy-tailed distribution; the negative skewness depicts left asymmetry (test) and right asymmetry (ABAQUS models).

5.3 Second shaking test: retrofitted model

The second shaking test, performed on the retrofitted adobe model, gives interesting results. The pdf and cdf distribution were obtained for accelerometers 1 and 2 for the ABAQUS and experiment data (second phase D = 60 mm). For accelerometer 1, the ABAQUS model is relatively close to the real data (pdf); the distribution shows symmetry in both curves and the cdf depicts close approximation (Figure 5.5).

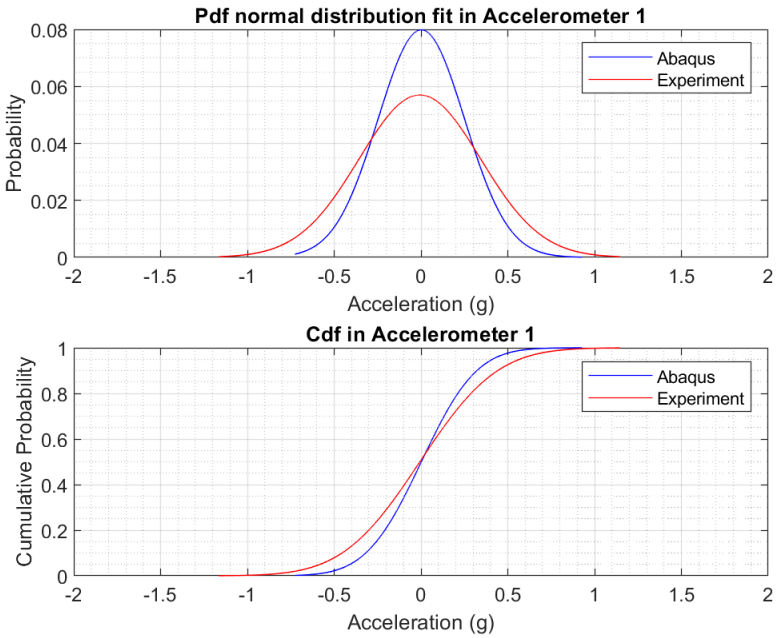

Figure 5.5. Shaking test on retrofitted structure: pdf and cdf for accelerometer 1 (ABAQUS and experimental data).

For accelerometer 2, the ABAQUS model provides a pdf distribution with values less than the observed ones (experiment). However, the cdf plot is similar for the ABAQUS and experiment data (Figure 5.6).

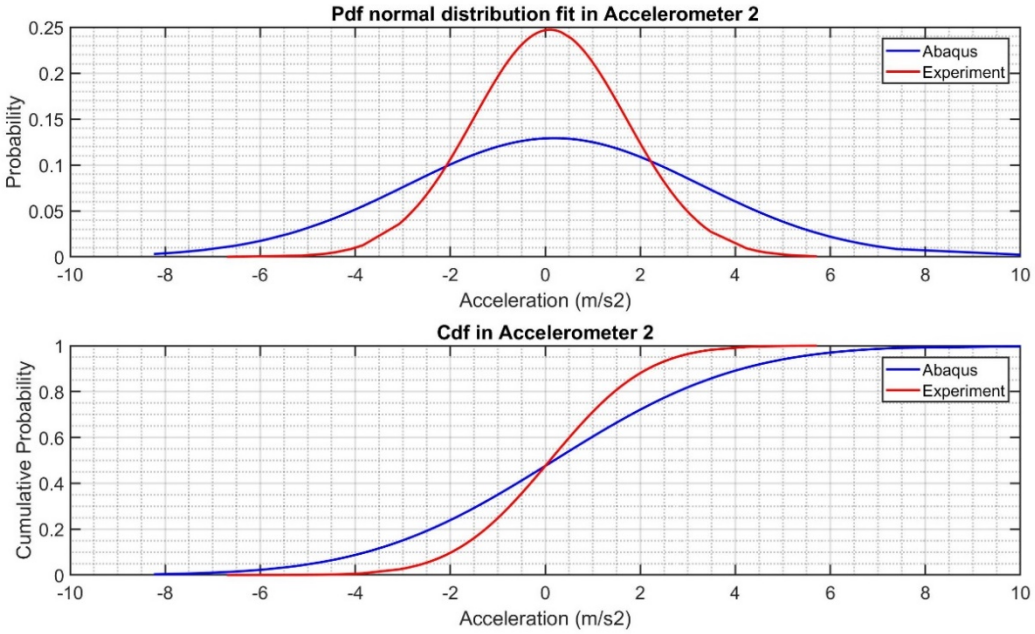

Figure 5.6. Shaking test on retrofitted structure: pdf and cdf for accelerometer 2 (ABAQUS and experimental data).

Accelerometers 1 and 2 show similar values for the pdf and cdf distribution provided that they are located at the top of the adobe full-scale model (lateral walls). After retrofitting and second shaking test, accelerometer 1 shows a similar behavior for pdf and cdf. However, accelerometer 2 shows an increment for the pdf values after the second shaking test. The difference among the real test data and the results from ABAQUS is due the fact that the model tries to simulate the nonlinear behavior of the adobe structure subjected to seismic behavior. Several issues should be considered such as the interaction among adobe blocks, the friction coefficient, the nonlinear properties of adobe material, and possible damage in the overall adobe structure.

Hence, accelerometers 1 and 2 provide similar statistics in ABAQUS compared to the ones obtained from the real experiment on the retrofitted adobe dwelling (Table 5.3).

Table 5.3. Statistics on accelerometers after seismic test on retrofitted model (phase 2)

Accelerometer	Acceleration		Statistics		
ID	Maximum (g)	Minimum (g)	Standard Dev. (g)	Skewness	Kurtosis Coeff. -3
A1 – Test	1.145	-1.165	0.350	-0.217	1.323
A2 - Test	0.653	-0.706	0.165	0.227	1.829
A1 - Abaqus	0.595	-0.578	0.191	0.090	0.964
A2 - Abaqus	1.252	-0.840	0.315	0.162	0.948

The ABAQUS model brings about a relative fair approximation for the real experiment. The Kurtosis coefficient depicts heavy-tailed distribution; positive skewness depicts right asymmetry.

6 WAVELET ANALYSIS

ABAQUS software brought about acceleration responses for all instruments locations related to the full-scaled adobe model for both the first and second shaking table test. Accelerometers 1 and 2, which are located at the top of the module and parallel to shaking direction are analyzed; accelerometer 1 is located at the right wall, and accelerometer 2 is located at the left one. The wavelet analysis considers the two seismic tests performed on the adobe model: First shaking test (phase 2 with D = 60 mm), and second shaking test (phase 2 with D = 60 mm).

6.1 Accelerometer 1

MATLAB provides the time-frequency representation of acceleration responses. The cone of influence, where edge effects are significant, is shown for both tests (Figure 6.1 and Figure 6.2). The Analytic CWT Scalogram was obtained by means of Morlet Wavelet transform.

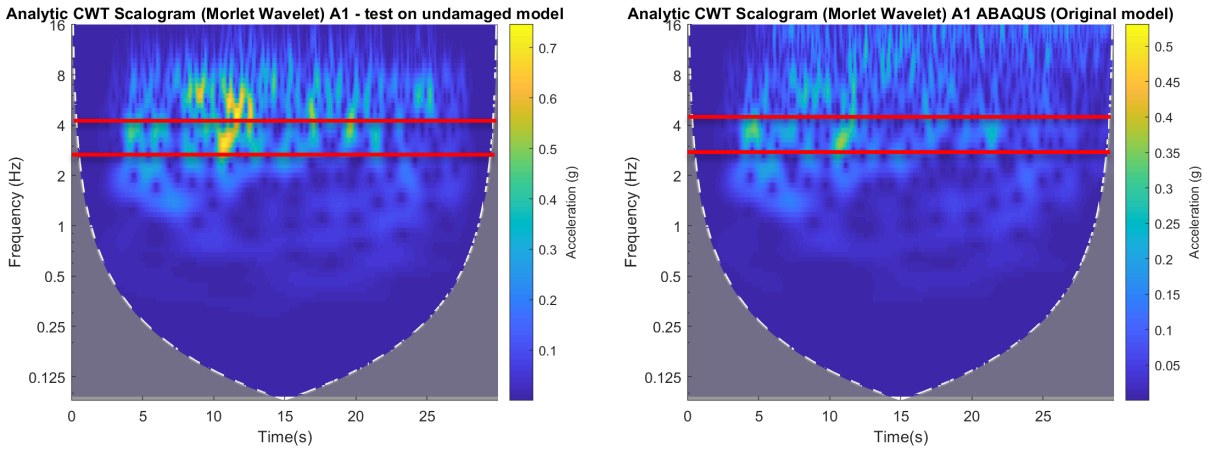

Figure 6.1. Analytic CWT for Accelerometer 1 (original model). Left: Experiment (phase 2, D = 60 mm). Right: ABAQUS simulation (phase 2, D = 60 mm).

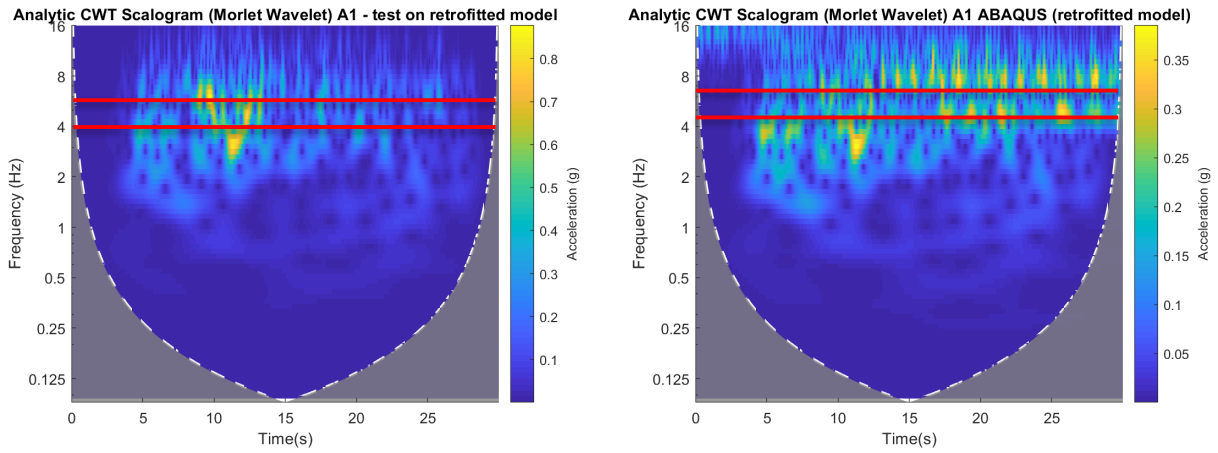

Figure 6.2. Analytic CWT for Accelerometer 1 (retrofitted model). Left: Experiment (phase 2, D = 60 mm). Right: ABAQUS simulation (phase 2, D = 60 mm).

The ABAQUS model detects the high frequency content with high acceleration located in the range 5 to 15 s (nearby f = 4 Hz). Provided that the software gives the estimated first mode (2.44 Hz) and sixth mode (4.17 Hz), the wavelet analysis proved to be effective in detecting the frequency content that occurs on the real test. Regarding the retrofitted model, the estimated first frequency (f = 4.54 Hz) is detected in both test and numerical simulation. The Continuous Wavelet Transform (CWT) shows a linear y-axis for comparison (Figure 6.3 and Figure 6.4).

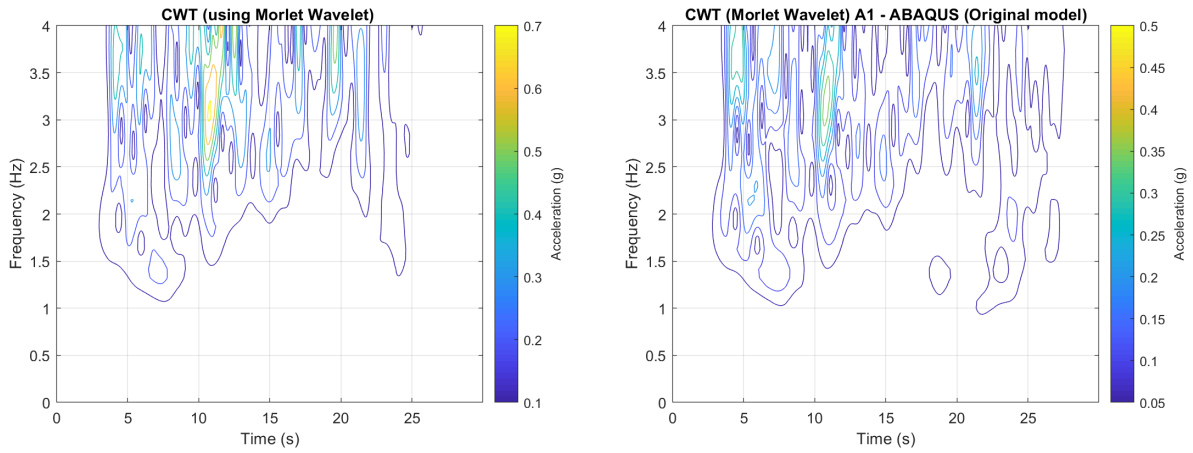

Figure 6.3. CWT for Accelerometer 1 (original model). Left: Experiment (phase 2, D = 60 mm). Right: ABAQUS simulation (phase 2, D = 60 mm).

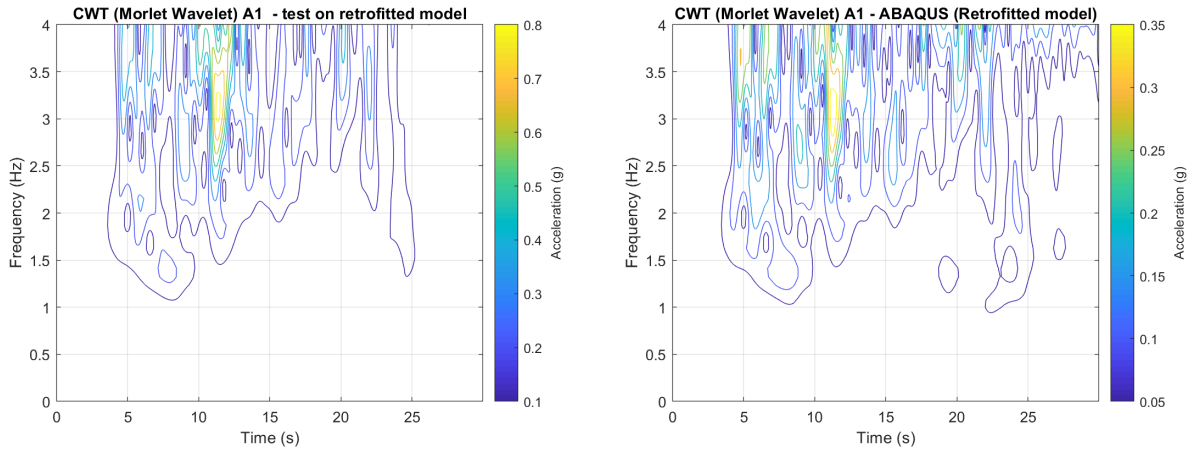

Figure 6.4. CWT for Accelerometer 1 (retrofitted model). Left: Experiment (phase 2, D = 60 mm). Right: ABAQUS simulation (phase 2, D = 60 mm).

6.2 Accelerometer 2

MATLAB provides the time-frequency representation of acceleration responses. The cone of influence (logarithmical border), where edge effects are significant, is shown for both tests in accelerometer 2 signal (Figure 6.5 and Figure 6.6). The Analytic CWT Scalogram was obtained by means of Morlet Wavelet transform.

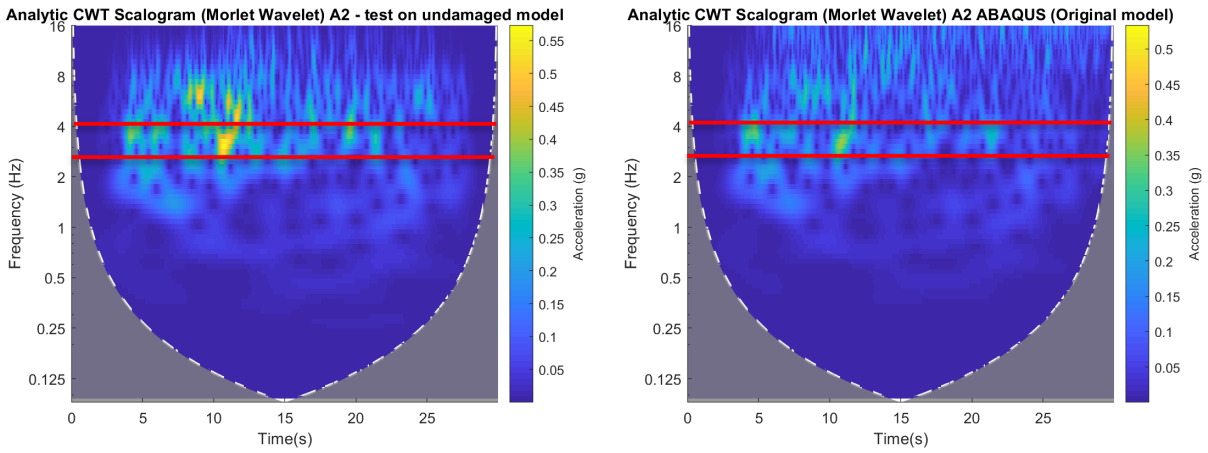

Figure 6.5. Analytic CWT for Accelerometer 2 (original model). Left: Experiment (phase 2, D = 60 mm). Right: ABAQUS simulation (phase 2, D = 60 mm).

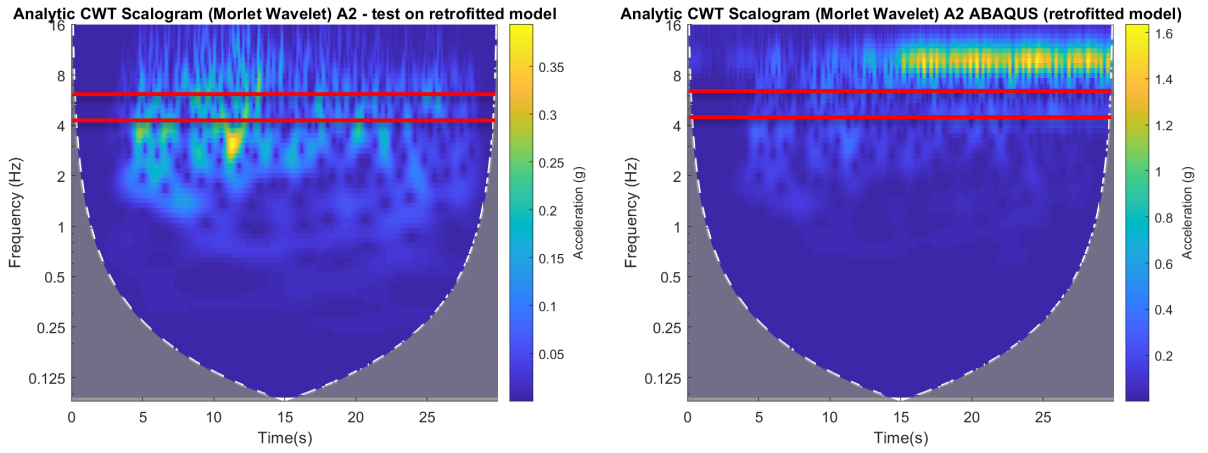

Figure 6.6. Analytic CWT for Accelerometer 2 (retrofitted model). Left: Experiment (phase 2, D = 60 mm). Right: ABAQUS simulation (phase 2, D = 60 mm).

The ABAQUS model detects the frequency content associated with high acceleration located in the range 5 to 20 s; this high content is located nearby f = 4 Hz. Provided that the estimated fifth (3.83 Hz) and sixth frequencies on the original model (4.17 Hz) are close to the observed frequency, the wavelet analysis proved to be effective in detect frequency content that occurs on the real test. Regarding the retrofitted model, the estimated first frequency (f = 4.54

Hz) is detected in the experiment. However, the numerical simulation in Accelerometer 2 does not approximate the test; it gives higher values for response acceleration. The Continuous Wavelet Transform (CWT) using Morlet Wavelet shows the detection of the frequency in a linear y-scale (Figure 6.7 and Figure 6.8).

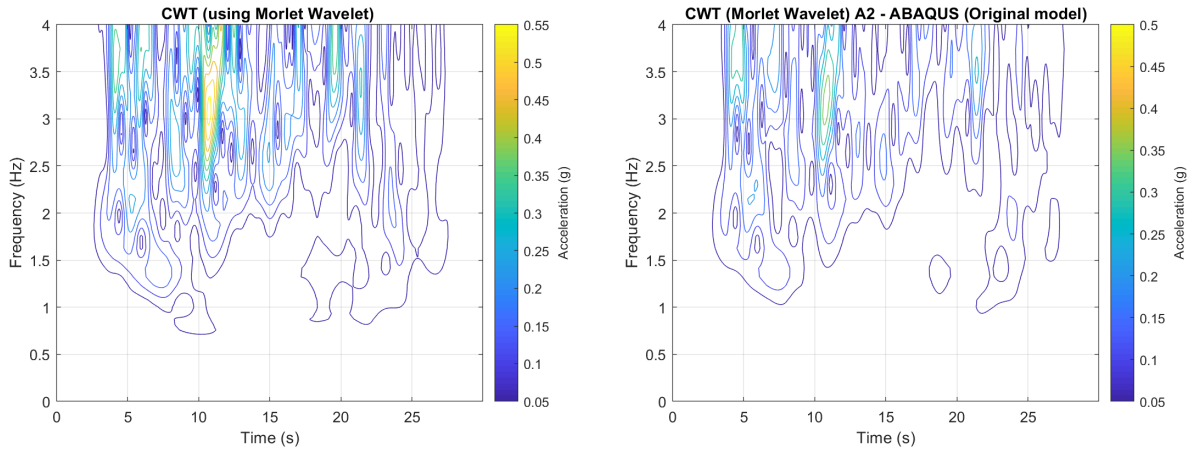

Figure 6.7. CWT for Accelerometer 2 (original model). Left: Experiment (phase 2, D = 60 mm). Right: ABAQUS simulation (phase 2, D = 60 mm).

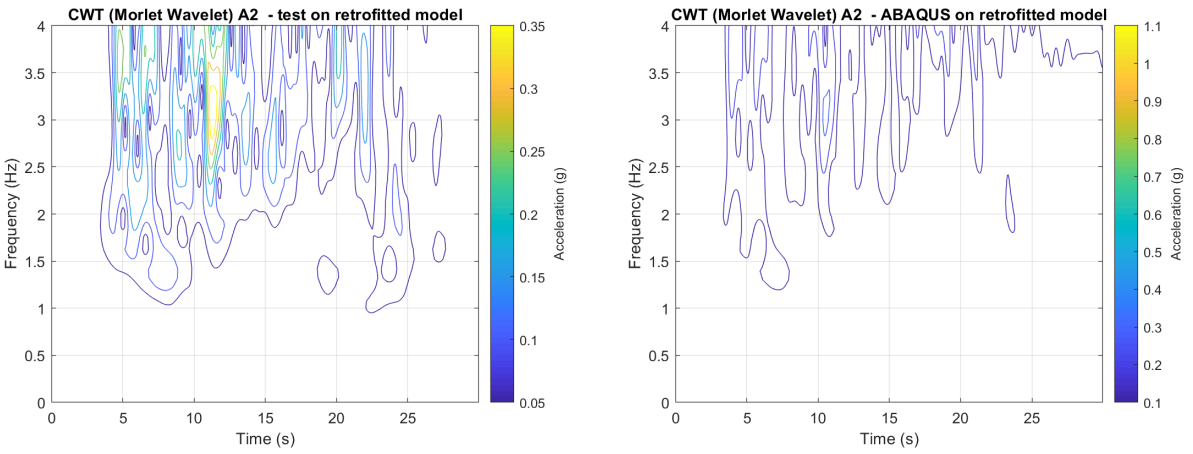

Figure 6.8. CWT for Accelerometer 2 (retrofitted model). Left: Experiment (phase 2, D = 60 mm). Right: ABAQUS simulation (phase 2, D = 60 mm).

The acceleration slightly changed after the test on the retrofitted model (0.50g to 0.35g) at f = 4 Hz level. The simulation shows an increment in the overall peak acceleration.

7 SUMMARY AND CONCLUSIONS

One and two story buildings constructed with adobe structures can be found in many countries throughout the world as noted in the introductory discussion. This research study was motivated by the students' interest in pursuing a topic relevant to his home country and the availability of time series data from a shake-table test of a full-scale one-story adobe structure conducted by Department of Civil Engineering at the Catholic University of Peru. This research investigation began with a literature review focused upon developing a better understanding of adobe as building material and it structural characteristics. The objective was to then use this information in order to develop a finite element model of the shake-table full scale structure and to compare its dynamic response characteristics for both the original undamaged structure and the repaired structure that were subject to the strong ground motion modeled in the experiment. In particular, two acceleration measurements at the same elevation on opposite wall were selected for analysis.

An accurate finite element model representation of a one-story adobe structure was quite involved as these structures consist of a concrete foundation, adobe walls and a timber roof. Constitutive nonlinear models for tension and compression used in the modeling of the adobe walls and linear models were used to characterize both the concrete and timber. ABAQUS models provide important tools needed to characterize the behavior of adobe structures subjected to seismic behavior. Block interaction can be represented in the software and output results such as displacements and accelerations can be predicted. The nonlinear behavior of adobe material should be carefully considered in any simulation, especially for the retrofitted model.

Statistical PDF and CDF distributions were used to compare numerical simulations with the experimental data. Further, cross-correlation was used in the comparison of two acceleration

signals, and the Root Mean Square Error (RMSE) was introduced to provide a measure of difference in two-time series. Wavelet analysis was introduced to provide new insights for both structural conditions allowing the detection of changes in frequency content with time. The results show a closer correlation for the original undamaged adobe structure. However, the Wavelet analysis for the retrofitted structure showed a discrepancy between the data and the model. These results highlight the difficulty in modeling buildings constructed using adobe especially when attempting to model damaged/retrofitted adobe structures. Some of the observed discrepancies can be attributed to the issues related to the material consistency and construction process. Thus, before attempting to predict the behavior of more complex adobe building structures such as a two-story adobe building more research focused on addressing adobe material variability and a better understanding of repair techniques and their modeling is required.

REFERENCES

[1.] ABAQUS (2018). “ABAQUS Documentation”, Dassault Systems, Providence, RI, USA.

[2.] Anderson, J. (2004) “Quantitative Measure of the Goodness-of-Fit of Synthetic Seismographs”. 13th World Conference on Earthquake Engineering 13WCEE2004, Vancouver, Canada, August 1st to 6th, 2004. Paper 243.

[3.] Alamdari, M., Samali, B., Li, J., Kalhori, H., Mustapha, S. (2006). “Spectral-Based Damage Identification in Structures under Ambient Vibration”. ASCE, Journal in Computing in Civil Engineering.

[4.] Bariola, J., and Sozen, M. (1990). “Seismic Tests of Adobe Walls”. Earthquake Spectra, Volume 6, No 4, pages 37-56. Earthquake Engineering Research Institute.

[5.] Barroso, L. (2017). “Advanced Dynamics and Control Structures Lecture Notes”. Texas A & M University, College Station, Texas.

[6.] Blondet, M., Tarque, N., and Acero, J., (2004). “Study of the Seismic Vulnerability of Nonengineered Buildings Located in the Peruvian Highlands (in Spanish)”. National Service for the Construction Industry Capacitation (SENCICO) and Catholic University of Peru (PUCP) joint project, Lima, Peru.

[7.] Blondet, M., Torrealva, D., Vargas, J., Velasquez, J. and Tarque, N. (2006) “Seismic Reinforcement of Adobe Houses Using External Polymer Mesh” (Procedure of the 1st European Conference on Earthquake Engineering and Seismology, Geneva, Switzerland.

[8.] Blondet, M., Vargas, J., Tarque, N., Soto, J., Sosa, C., and Sarmiento, J. (2017) “Seismic Reinforcement of Earthen Constructions”. 16th World Conference on Earthquake Engineering 16WCEE2017, Santiago Chile, January 9th to 13th.

[9.] Boroschek, R., and Comte, D. (2004). “Time Frequency Characteristics of the 2001 Peruvian (Mw= 8.40 Earthquake)”. 13th World Conference on Earthquake Engineering. Vancouver, Canada. Paper No. 287.

[10.] Bossio, S. (2010). “Evaluation of the Seismic Behavior and Movement Direction Influence of Adobe Models Reinforced with Geogrid (in Spanish).” Pontificia Universidad Catolica del Peru.

[11.] Bradford, C., Yang. J., and Heaton, T. (2006). “Variations in the Dynamic Properties of Structures: The Wigner-Ville Distribution”. Proceedings of the 8th US National Conference on Earthquake Engineering. April 2006, San Francisco, California, Paper 1439.

[12.] Chopra, A. (2007). “Dynamics of Structures”. University of California, Berkeley. 3rd edition. Pearson Education Inc.

[13.] Cline, D. (2017). “Statistical Analysis Lecture Notes”. Texas A & M University, College Station, Texas.

[14.] Clough, R., and Penzien, J. (1995). “Dynamics of Structures”. Computers & Structures, Inc., Berkeley, California. 3rd edition.

[15.] Cooper, G. R. J. (2016). “Attribute Based-Time Series Cross Correlation Measures” Pure and Applied Geophysics. Page 173 (2016), 1683-1702.

[16.] Freedman, D., Pisani, R., Purver, R., and Adbikari, A. 2007. “Statistics: An Excellent Introduction to Statistical Thinking, Requiring Minimal Mathematical Background” Norton, New York, 4th edition.

[17.] Gaviria, C., and Montejo, L. (2017). “Optimum Wavelet Parameters for System Identification of Civil Engineering Structures”. Earthquake Spectra. Earthquake Engineering Research Institute.

[18.] Ghodrati, G., Bagheri, A., and Seyed Razaghi, S. (2009) “Generation of Multiple Earthquake Accelerograms Compatible with Spectrum Via the Wavelet Packet Transform and Stochastic Neural Networks”. Journal of Earthquake Engineering, Volume 13, Issue 7.

[19.] Grossman, A., and Morlet, J. (1984). “Decomposition of Hardy Functions into Square Integrable Wavelets of Constant Shape”. SIAM J. Math.

[20.] Kumar, A. (2002). Rural Mud House with Pitched Roof, Report 23 (India).

[21.] Li H., Yi T., Gu M., and Huo L. (2009). Evaluation of Earthquake Induced Structural Damages using Wavelet Transform. Progress in Natural Science. (2009) Pages. 461-470.

[22.] Mattson, E. (2015). “Improved Seismic Resistant Design of Adobe Houses in Vulnerable Areas in Peru.” Uppsala University, Sweeden.

[23.] Montejo, L., Suarez, L. 2006. “Wavelet-Based Identification of Site Frequencies from Earthquake Records.” Journal of Earthquake Engineering, Volume 10, Issue 4 (2006) 565 - 594.

[24.] Montgomery, D., Runger, G. (2017). “Applied Statistics and Probability for Engineers.” Sixth edition. WILEY.

[25.] Newland, D.E. (1996). “An Introduction to Random Vibrations, Spectral and Wavelet Analysis.” Third edition, Longman Scientific and Technical, UK, John Wiley and Sons, NY.

[26.] Politis, N. (2000). “Advanced Time Frequency Applications in Earthquake Engineering”. Seismic Design and Analysis of Structures. Department of Civil Engineering. Rice University.

[27.] Rathje, E., Abrahamson, N., and Bray, J. (1998). “Simplified Frequency Content Estimates of Earthquake Ground Motions”. Journal of Geotechnical and Geothermical Engineering, pages 150-159.

[28.] Rathje, E., Abrahamson, N., and Bray, J. (2004). “Empirical Relationships for Frequency Content Parameters for Earthquake Ground Motions”. Earthquake Spectra, Volume 20, No 4, pages 119-144. Earthquake Engineering Research Institute.

[29.] Saragoni, G., Astroza, M., and Ruiz, S. (2004). “Comparative Study of Subduction Earthquake Ground Motion of North, Central and South America.” 13th World Conference on Earthquake Engineering. Vancouver, Canada. Paper No. 287.

[30.] Silveira, D., Varum, H., Costa, A., and Carvalho, J. (2015). “Mechanical Properties and Behavior of Traditional Adobe Wall Panels on the Aveiro District”. Journal of Materials in Civil Engineering, 2015, 27 (9),

[31.] Sokolov, V. (2002). “Seismic Intensity and Fourier Acceleration Spectra: Revised Relationship”. Earthquake Spectra, Volume 18, No 1, pages 161-187. Earthquake Engineering Research Institute.

[32.] Tarque, N., Camata, G., Spacone, E., Varum, H. and Blondet, M. (2014). "Nonlinear Dynamic Analysis of a Full-Scale Unreinforced Adobe Building". Earthquake Spectra, Volume 30, No 4, pages 1643-1661. Earthquake Engineering Research Institute.

[33.] Torrence, C., and Compo, G. (1998). “A Practical Guide to Wavelet Analysis.” Bulletin of the American Meteorological Society.